
MODELING SURRENDER RISK IN LIFE INSURANCE: THEORETICAL AND EXPERIMENTAL INSIGHT

Mark Kiermayer

Department of Natural Science
University of Applied Sciences Ruhr West
mark.kiermayer@hs-ruhrwest.de

January 28, 2021

ABSTRACT

Surrender poses one of the major risks to life insurance and a sound modeling of its true probability has direct implication on the risk capital demanded by the Solvency II directive. We add to the existing literature by performing extensive experiments that present highly practical results for various modeling approaches, including XGBoost and neural networks. Further, we detect shortcomings of prevalent model assessments, which are in essence based on a confusion matrix. Our results indicate that accurate label predictions and a sound modeling of the true probability can be opposing objectives. We illustrate this with the example of resampling. While resampling is capable of improving label prediction in rare event settings, such as surrender, and thus is commonly applied, we show theoretically and numerically that models trained on resampled data predict significantly biased event probabilities. Following a probabilistic perspective on surrender, we further propose time-dependent confidence bands on predicted mean surrender rates as a complementary assessment and demonstrate its benefit. This evaluation takes a very practical, going concern perspective, which respects that the composition of a portfolio might change over time.

Keywords confidence predictions, confidence bands, resampling, ensemble techniques, neural networks, XGBoost

1 Introduction

Managing risks is at the core of insurance business. With the publication of the Solvency II directive in 2009 European insurers are required to work towards a holistic view of risk. In particular, it states individual modules for the underwriting risk, market risk and counterparty default risk. For life insurance business, the Solvency II directive requires the underwriting risk to explicitly indicate the risk of individual sub-components like mortality, longevity, morbidity, life-expense, revision, lapse and life-catastrophe. In the German market, traditional risks as mortality and longevity are generally addressed by using safety buffers on mortality assumptions, see e.g. the German 2008T and 2004R tables, as well as its comparison to international approaches in [12]. The present work looks at a sound estimation of surrender risk. We place a particular focus on the distributional effect of resampling schemes that are commonly used to mitigate the rare event character of surrender.

Lapse risk has been identified as a major risk to life insurance business by the Quantitative Impact Study QIS5 of the European Insurance and Occupational Pensions Authority and related research, see e.g. [5, 33]. In [18], lapse

risk is officially defined as "all legal or contractual policyholder options which can significantly change the value of the future cash-flows". Hence, lapse risk includes not only a premature and full termination of contracts, but for example also partial terminations, changes to the frequency or quantity of premium payments, altered benefits or extension of coverage. For accuracy, we use the term *surrender* to specifically refer to a premature, full termination of a contract induced by the policyholder. Colloquially, however, surrender and lapse are often used interchangeably. Overall, the effects of surrender are manifold. Arguably most harmful to the insurer are early surrenders that cost the insurer its initial expenses or adverse selection that alters the composition of the portfolio and compromises a sound diversification. The review in [16] provides an extensive overview of past research on surrender risk and divides the respective literature into two subsets. Given a theoretical framework, we can determine a fair value estimate of the embedded options, see e.g. [5, 33, 34]. This theoretical perspective is not limited to risk-neutral individuals, but can be extended to risk-avers and non-rational consumer behavior, see [16]. On the other hand, there exists extensive empirical research, which aims to identify the main risk drivers for lapse events and to test for modeling hypotheses, as well as the quality of modeling approaches to capture the underlying risk, see e.g. [2, 7, 15, 29, 41, 52]. The most common modeling classes include logistic regressions and tree based methods as CART and random forests, where the evaluation is typically performed with metrics on the respective confusion matrix or the related receiver operating curve (ROC) for assessment and model choice. The work in [2, 7, 37, 38] indicate how the quality of empirical lapse models translates to economic measures. In [4] we see the inclusion of contagion effects in the modeling of lapse risk. We note that the majority of empirical modeling approaches focus on a single-period lapse prediction, which is to a large extent motivated by the one-year $\text{VaR}_{0.995}$ risk measure imposed by the Solvency II directive. A multi-period perspective on lapse dynamics including a proposition for lapse tables, that can be used in similar fashion to standard mortality tables, can be found in [40]. The authors of [40] apply survival analytical methods, as e.g. the Fine&Gray model, see [20], in order to distinguish between competing risks that can lead to the termination of a contract.

In the present work, we provide extensive numerical experiments that investigate the quality of common modeling approaches for surrender risk, namely logistic regression, tree based methods and neural networks, each in a bagged and a boosted version. All models are analyzed on four different portfolios of endowment policies, each showing surrender behaviours that replicate findings reported in the literature, see [8, 15, 41]. Overall, we find highly competitive results, where XGBoost consistently displays superior performance. For model evaluation, we look at the latent, true surrender probabilities, as well as observable realizations of surrender events. Accessing the true probabilities allows us to determine the exact bias and variance and monitor whether accessible concepts for model assessment reliably capture the latent dynamics of surrender. In view of the bias of a model, our results indicate a conflict between accurate label predictions and sound confidence predictions. We illustrate this with the example of resampling, which is commonly used to obtain more accurate label prediction of the minority class. Although, we can confirm common resampling techniques to improve the F_1 -score, we theoretically and numerically show that resampling comes at the cost of a significant bias of estimated surrender probabilities. Following this probabilistic perspective, we introduce time-dependent confidence bands for the predicted mean surrender rate as an alternative evaluation, which indicate the uncertainty of predicted surrender probabilities. This allows us to assess the quality of a model from a very practical going concern perspective, where the composition of the underlying portfolio and the predominant risk drivers might change over time. In particular, confidence bands highlight that adding a risk buffer to a naive baseline does not cover the surrender risk sufficiently.

The remainder of this paper is organized as follows. We start by clarifying the objective in Section 2. In Section 3, we review common, frequentistic concepts to evaluate binary classifiers and contrast them to probabilistic alternatives. Next, in Section 4 we discuss the rare event setting of surrender risk and analyze the distributional effect of common resampling methods. Section 5 presents the simulation and preparation of all data used in our numerical experiments. In Section 6, we then describe the specific parameterization of all classifiers and report numerical results. Lastly, we conclude in Section 7 with an outlook for future work.

2 Objective

Let the probability space $(\Omega, \mathcal{F}, \mathbb{P})$ describe our stochastic environment. We denote an arbitrary insurance contract at time $t \in \mathbb{N}_0$ by $X_t : \Omega \rightarrow \mathbb{R}^n$, $n \in \mathbb{N}$. The time series $(X_0, X_1, X_2, \dots, X_T)$ then represents the evolution of the contract up to the random period of termination $T : \Omega \rightarrow \mathbb{N}_{\geq 0}$, recording e.g. the age of the policyholder or the assured benefits. As the termination can have multiple causes, like surrender, death or maturity, we record the respective state at the end of period t by $J_t : \Omega \rightarrow \mathbb{N}_0$, where $J_t = 0$ for $t = 0, \dots, T-1$ indicates an active contract. All states $J_T \in \mathbb{N}$ are terminal, absorbing states. They describe competing, censoring events, in the sense that observing $\{J_T = i\}$ and $\{J_T = j\}$, $i \neq j$, are mutually exclusive, both end the observation on the time series and prevent a realization of an alternative state. For more detail on censoring and competing risks we refer the reader to [1].

Single period setting. In this work we consider three terminal states, namely surrender, death and maturity. Surrender is represented by $\{J_T = 1\}$. Death and maturity are indicated by $\{J_T = 2\}$ and $\{J_T = 3\}$, but will not be modeled explicitly. Further, in line with the Solvency II directive, we focus on a single period setting. Hence, we define targets Y_t by $Y_t := \mathbb{1}_{\{J_t=1\}}$. Given a realization x_t of X_t , our objective is to estimate the probability of the active contract x_t to surrender within the period $[t, t+1]$, i.e. to obtain an estimate for the conditional probability

$$p(1|x_t) := \mathbb{P}(Y_t = 1|X_t = x_t), \quad (1)$$

or, equivalently, to model the random variable

$$Y_t|(X_t = x_t) \sim \text{Ber}(p(1|x_t)). \quad (2)$$

It is important to note that (1) implicitly imposes the Markov property that the random state J_t and the past represented by $X_{t-k} = x_{t-k}$ are independent for $k = 1, \dots, t$. In the literature, it is common to assume that the time horizon influencing surrender decisions of policyholders is restricted to one period, see e.g. [2, 41]. Also, conditioning on an active contract x_t concurrently implies $T \geq t$.

Overall, our objective is a common setup for supervised learning, where we aim to obtain a model $\hat{p} : \mathbb{R}^n \rightarrow [0, 1]$, $x \mapsto \hat{p}(1|x)$, such that it minimizes the loss function $\ell : [0, 1] \times \{0, 1\} \rightarrow \mathbb{R}$, i.e.

$$\hat{p} := \underset{\bar{p}}{\text{argmin}} \ell(\bar{p}(1|X_t), Y_t). \quad (3)$$

We would like to draw attention to the non-binary output of the model \hat{p} . The contrast between binary and non-binary prediction will be a major topic throughout this paper. In the style of [45], we call estimates $\hat{p}(1|x_t) \in [0, 1]$ *confidence prediction*. In contrast, we refer to binary predictions $\hat{y}_t \in \{0, 1\}$, that purely focus on the realization of $Y_t|(X_t = x_t)$, as *label predictions*. Naturally, any confidence prediction $\hat{p}(1|x_t)$ can be transformed to a label prediction based on some threshold $c \in [0, 1]$, i.e. $\hat{y}_t = \mathbb{1}_{\{\hat{p}(1|x_t) \geq c\}}$.

In practice, obtaining a sound model \hat{p} is complicated by the rare event character of surrender. We discuss rare events separately in Section 4, with a specific focus on their effect on confidence predictions and the distributional effect of common resampling strategies. First, we would like to conclude this section by commenting on the setting at hand and review approaches to evaluate classifiers in Section 3.

Context for alternative settings. The presented objective is customized to the Solvency II directive and a one-year perspective, which disregards the exact time of surrender within the year. Other settings, e.g. a risk neutral product design, might ask for a more general setup where the risk of individual events $\{J_T = i\}$, $i \in \mathbb{N}_0$, are estimated jointly in a multi-period setting. In particular, this requires a more general, real-valued random event $T : \Omega \rightarrow \mathbb{R}_{\geq 0}$ and random state variable $J_t : \Omega \rightarrow \mathbb{N}_0$, $0 \leq t \leq T$. Given a realization x_t of X_t , the objective then changes to estimating the *cause-specific hazard rate* $\alpha_{T,i}(\tilde{t}|x_t)$ of the terminal events $i \in J_t(\Omega)$ at time $\tilde{t} \geq t$. According to [1], the quantity $\alpha_{T,i}(\tilde{t}|x_t)$ is defined by

$$\alpha_{T,i}(\tilde{t}|x_t) := \lim_{\Delta \rightarrow 0} \frac{1}{\Delta} \mathbb{P}(\tilde{t} \leq T \leq \tilde{t} + \Delta, J_T = i | T \geq \tilde{t}, x_t). \quad (4)$$

Note that conditioning on an active contract x_t also implies that $J_{\tilde{t}} = 0$ for all $\tilde{t} < t$, as in our context all states $J_{\tilde{t}} \neq 0$ are terminal and competing risks. For a detailed discussion of $\alpha_{T,i}(\tilde{t}|x_t)$ and its estimation we refer the reader to [1, 40]. Instead we want to comment on the practical implications of (1) and (4).

Quantities in (4) can be thought of as time-dependent transition intensities from the active state 0 to a terminal state i in a Markov model. Cause-specific hazard rates provide a more detailed insight into the likelihood of states J_T to be realized and might be used to form a table for lapse probabilities, see e.g. [40]. It is well known that simply ignoring competing risks, as e.g. death or maturity for surrender, alters the estimated hazards $\alpha_{T,i}(\tilde{t}|x_t)$, which are asymptotically unbiased, see e.g. Section 3.4 in [1]. On the other hand, modeling a Bernoulli variable as in (1) translates to asking how likely is it to observe a surrender event of contract x_t within the next period. Here, all non-surrender states $J_t \neq 1$ are combined by introducing the target Y_t . Further, in our one-period perspective we have complete observations as either surrender or non-surrender is realized. In contrast, if we do not observe contract x entering a terminal state $J_T > 0$, the observation on x yields a right-censoring event for the estimation of (4).

For notational convenience, in the remainder of this work we drop the time index t in (X_t, Y_t) and denote realizations $(x, y) \sim (X, Y)$ by the use of small letters. The progression of time is implicitly recorded by features like the age of the policyholder. Consequently, we denote the true surrender probability of realization x by $p(1|x)$, the confidence prediction by $\hat{p}(1|x)$ and the label prediction by \hat{y} . In the following, we use indices to count data in our data set, e.g. x_k , and exponents, if we explicitly want to refer to components, e.g. $x_k^{(j)}$.

3 Model evaluation

Usually, binary classifiers are evaluated based on their label predictions. In this section, we review classical approaches for evaluating classifiers, discuss shortcomings of their frequentistic focus and provide probabilistic alternatives. Our reasoning is dictated by the objective of sound confidence predictions, in contrast to accurate binary label predictions to model actions or definite class memberships.

Frequentistic evaluation. In a binary classification task, the label prediction \hat{y} for a record x with label y can either be true, i.e. $\hat{y} = y$, or false, i.e. $\hat{y} \neq y$. Based on whether the prediction \hat{y} is positive ($\hat{y} = 1$) or negative ($\hat{y} = 0$), we refer to a prediction as true, respectively false, positive or negative. A common evaluation is to present the count of all predictions \hat{y} w.r.t. their correct label y in a 2×2 matrix, a so-called *confusion matrix*, see [2, 19, 41]. We provide an illustration of a confusion matrix in the Appendix A.4, see Figure 6. Based on the absolute frequencies in a confusion matrix, we can then formulate a variety of performance measures. Common examples include, accuracy, precision, recall, specificity or F_β -score for $\beta > 0$. Table 3 in the Appendix A.5 summarizes the definition of well-known performance measures.

We argue that a confusion matrix, and respective performance measures, do not provide a sound evaluation. Most performance measures solely look at individual aspects of our classifier and individually provide a deficient evaluation as they are invariant towards specific changes in the confusion matrix. For example, precision or specificity each disregards either label prediction of type $\hat{y} = 0$ or data labeled with $y = 1$ all together. On the other hand, accuracy simultaneously measures correct classifications for both classes $y \in \{0, 1\}$, however, has little explanatory power when there is an imbalance between data with label $y = 0$ and $y = 1$. For imbalanced data a naive prediction of exclusively the majority class will indicate a particularly high accuracy if data of the minority class is very rare. Similarly, the F_β -score takes a broader perspective by quantifying the trade-off between precision and recall, yet is invariant to the count of correct predictions $\hat{y} = 0$. A more detailed analysis of individual performance measures, with a particular focus on invariance under permutations in the confusion matrix, is provided in [47]. At the core of our critic lies the use label predictions, given a probabilistic objective. For confidence predictions $p(1|x) \in [0, 1]$, the underlying confusion matrix is based on a single threshold c for label predictions $\hat{y} = \mathbb{1}_{\{p(1|x) > c\}}$. This implies that

our evaluation is highly insensitive towards changes in $p(1|x)$.

One way to examine a classifier's performance more holistically is check how performance measures change for varying values of $c \in [0, 1]$. A common choice is to look at the trade-off between recall, alias true positive rate, and false positive rate. The resulting tuples can be plotted in $[0, 1]^2$ and the result is known as the *receiver operating characteristics* (ROC) curve. Note that recall and false positive rate are intertwined in a way that randomly classifying the share $p \in [0, 1]$ of all records as positive, i.e. $\hat{y} = 1$, results in an expected recall and false positive rate of p . Hence, a ROC curve above the diagonal in $[0, 1]^2$ indicates the classifier to perform better than random guessing. The notion of 'better' is formalized by the *area under curve* (AUC), the integral of the ROC on $[0, 1]$, where $\text{AUC} > 0.5$ indicates a classifier superior to random guessing. Alternatively, the *convex hull* of the ROC curve can be utilized to determine optimal values of c or even to compare different classifiers, see e.g. [19, 43].

Although ROC and its AUC are common evaluations, we note that recall and false positive rate each focus on the evaluation of one label. Thus, a ROC approach is independent of the relative frequency of the two classes $y = 0$ and $y = 1$, i.e. insensitive to imbalanced data. The *precision-recall curve* presents an alternative model evaluation, which follows the same logic as ROC, see [19]. However, the precision considers both actual labels, $y = 0$ and $y = 1$, and therefore is sensitive to the balance of data.

Even when looking at multiple thresholds c simultaneously, the discussed frequentistic performance measures evaluate binary label predictions. In the very simplistic example of constant surrender rates, i.e. $p(1|x) \equiv p$, which we assume to model perfectly, i.e. $\hat{p}(1|x) \equiv p$, any label prediction $\hat{y} = \mathbb{1}_{\{\hat{p}(1|x) \geq c\}}$, $c \in [0, 1]$, predicts only one outcome for all observations x . In order to avoid this loss of information, we look at more probabilistic measures of performance.

Probabilistic evaluation. Ideally, we would like to compare the confidence predictions $\hat{p}(1|x)$ with true event probabilities $p(1|x)$, e.g. by employing standard p-q plots. Given data $\{(x_i, y_i)\}_{i=1}^N$, we denote the mean absolute difference of these quantities by

$$\text{mae}(p, \hat{p}) := \frac{1}{N} \sum_i |p(1|x_i) - \hat{p}(1|x_i)|. \quad (5)$$

In our experiments, we construct a setup where we can access the true surrender probabilities $p(1|x)$, in order to look at the model fit from a probabilistic point of view. However, this is a purely theoretical perspective as in practice we do not observe $p(1|x)$ but only the binary realization y from $\text{Ber}(p(1|x))$. Thus, information theory provides a more practical approach. One can show that the maximum likelihood estimator $\hat{p}(1|x)$ corresponds to minimizing the Kullback-Leibler divergence, respectively equivalently minimizing the cross-entropy, see [25]. Using standard notation, we denote the empirical estimate of the (binary) cross-entropy by

$$H(\hat{p}) := -\frac{1}{N} \sum_i y_i \log \hat{p}(1|x_i) + (1 - y_i) \log (1 - \hat{p}(1|x_i)). \quad (6)$$

Hence, minimizing the binary cross-entropy provides a maximum-likelihood consistent estimator, which is why the cross-entropy is the most commonly chosen loss function in classification. Unfortunately however, the cross-entropy lacks a comprehensive, practical interpretation for surrender. Therefore, we introduce a third option to evaluate confidence predictions, based on the central limit theorem of Lindeberg-Feller, see e.g. [32], Theorem 15.43.

Proposition 1. Let x_1, \dots, x_N be realizations of contract X . Let Z_1, \dots, Z_N describe random, independent surrender event, where $Z_i \sim \text{Ber}(p(1|x_i))$, $i = 1, \dots, N$. Then, if there exists $\varepsilon > 0$ such that $p(1|x) \in [\varepsilon, 1 - \varepsilon]$ for any contract $x \sim X$, then

$$\frac{1}{\sigma(S_N)} \sum_i Z_i - p(1|x_i) \xrightarrow{d} \mathcal{N}(0, 1), \quad N \rightarrow \infty, \quad (7)$$

with

$$\sigma(S_N) := \sqrt{\text{Var} \left(\sum_i Z_i \right)} = \sqrt{\sum_i p(1|x_i)(1 - p(1|x_i))} \quad (8)$$

holds.

Proof. See Appendix A.1.

Assuming $Z_i := (Y|X = x_i)$ in Proposition 1 to be independent means that, given circumstances x_i , policyholders act independently of each other. If x_1 and x_2 present observations on the same contract, i.e. the same policyholder, at different times this assumption is implausible. Hence, in application we restrict x_i in Proposition 1 to stem from the portfolio of the insurer for a fixed calendar year. Features that can effect the surrender risk of all policyholders holistically, as e.g. rising interest rate, can be recorded as a component of contracts x_i . Thus, a holistic increase of the surrender risk does not violate the independence of surrender decisions Z_i . Note that the technical restriction of $p(1|x_i) \in [\varepsilon, 1 - \varepsilon]$ does not impact the asymptotic distribution in Proposition 1. We can think of it as assuming a minimum risk for surrender and non-surrender. For any finite data set $\{(x_i, y_i)\}_{i=1}^N$ with estimator $\hat{p}(1|x_i) \in (0, 1)$ there exists $\varepsilon > 0$ which satisfies $\hat{p}(1|x_i) \in [\varepsilon, 1 - \varepsilon]$.

Corollary 1. Let the assumptions of Proposition 1 hold and let $\hat{p} : x \mapsto \hat{p}(1|x)$ denote an estimator of $p(1|x)$. Given the confidence level $\alpha \in (0, 1)$, we can then construct a confidence interval for the mean surrender rate by

$$\left(\frac{1}{N} \sum_i \hat{p}(1|x_i) \right) \pm z_{1-\alpha/2} \frac{\sqrt{\sum_i \hat{p}(1|x_i)(1 - \hat{p}(1|x_i))}}{\sqrt{N(N-1)}}, \quad (9)$$

where $\hat{p}(1|x_i)$ presents the model estimate for $p(1|x_i)$ and $z_{1-\alpha/2}$ the respective percentile of the standard normal distribution. The best point estimate for the mean surrender rate is given by $\frac{1}{N} \sum_i \hat{p}(1|x_i)$.

Proof. See Appendix A.1.

If we were to work with label predictions $\hat{y}_i := \mathbb{1}_{\{\hat{p}(1|x_i) \geq 0.5\}} \in \{0, 1\}$, the quantity $\frac{1}{N} \sum_i \hat{y}_i$ also provides an estimator for $\mathbb{E} \left(\frac{1}{N} \sum_i Z_i \right)$. However, without an estimate of the distribution of Z_i we cannot express any level of confidence for our predictions. In Section 6, we apply Corollary 1 for each calendar year separately and obtain confidence bands on our time series. This approach relaxes the assumptions of [41], where the authors construct confidence intervals under the assumption of homogeneous and identically distributed subgroups of contracts.

4 Rare events

We now combine the nature of rare events with the objective of Section 2 and look at the effect of frequentistic performance measures in view of the probabilistic objective. We start with a definition of rare events, motivate resampling and examine it from a purely theoretical point of view. Thereafter, we interpret these results for common classifiers in practice.

In binary classification, we generally refer to data $\{(x_i, y_i)\}_{i=1}^N$ drawn from (X, Y) as *balanced data* if both classes contain about equally many observations, i.e. $\sum_i y_i \approx \sum_i (1 - y_i)$. As this heuristic definition refers to the data itself, data imbalance might be introduced during the collection of data. Concerns about biased collection of data are discussed e.g. in [30]. Overall, it has been widely acknowledged in literature, see [39, 46, 49, 50], that imbalanced data can lead to classifiers which are biased towards predicting the majority class, and that standard metrics, as e.g. accuracy, are inappropriate. Here, the notion of a bias refers solely to label predictions. In the particular case of the logistic regression imbalanced data leads to low values in the Hessian matrix, see [26]. Hence, estimated regression parameters are highly unstable, despite being asymptotically unbiased.

In contrast to imbalanced data, we characterize *rare events* by their low, true probability $\mathbb{P}(Y = 1) < \varepsilon$, where the value of ε can be domain specific, see [44]. In practice, values as low as $\varepsilon = 0.05$ or $\varepsilon = 0.01$ are commonly found in e.g. surrender of insurance contracts [2, 40, 41] or fraud detection [36, 42]. In this work, we will assume perfect data in the sense that any imbalance between surrender and non-surrender events stems from the rare event character of the task at hand and is not the consequence of improper data collection.

To address the concern of biased classifiers on imbalanced data, the literature proposes two main techniques, cost-sensitive-learning and resampling, see e.g. [17, 30, 39, 46, 49, 50]. Both have empirically shown to be capable of improving classifiers regarding their recall, F_β , AUC or geometric mean of the true positive and true negative rate, see e.g. [10, 46, 49, 51]. In [45], we see that popular boosting schemes like 'AdaBoost' can be also interpreted as an adaptive resampling. For completeness we note that, research in data mining indicates that classifiers can also benefit from removing outliers or accounting for noisy measurements close to the decision boundary. For a more comprehensive review we refer the reader to [9, 27]. In the following, we focus on common resampling schemes, as resampling data and applying weights to the empirical loss function are conceptually equivalent. This argument is supported by the authors in [49], who yet contend that sampling approaches will generally outperform cost sensitive learning.

We start with a purely theoretical perspective on resampling. Therefor, we denote the marginal, respectively joint, density functions of (X, Y) at (x, y) by $p(x)$ and $p(y)$, respectively $p(x, y)$. Note that the specific letter indicates the underlying random vector as it is common in Bayesian literature, see e.g. [48]. Further, we introduce the functions

$$p(y|x) := \begin{cases} p(x, y) / p(x), & p(x) > 0 \\ 0, & p(x) = 0, \end{cases} \quad p(x|y) := \begin{cases} p(x, y) / p(y), & p(y) > 0 \\ 0, & p(y) = 0. \end{cases} \quad (10)$$

Based on the concept of regular conditional distributions, see [14, 32], both functions in (10) are well defined on the given probability space $(\Omega, \mathcal{F}, \mathbb{P})$ as a function w.r.t. either x or y . Hence, we are justified to interpret $p(y|x)$ as a conditional density given the condition x or as a measurable function w.r.t. its condition x .

Heuristically, over- or undersampling aim to mitigate the imbalance between classes by either dropping samples of the majority class or resampling samples from the minority class. We call this procedure *random over-* respectively *undersampling* if the resampling respectively dropping is performed randomly. In practice, these sampling procedures are usually performed until the data is balanced, as illustrated in the following example.

Example 1 (Random resampling). Let us assume two random variables $G, K : \Omega \rightarrow \mathbb{R}^n$, $n \in \mathbb{N}$, that present two different events. In terms of previous notation, we can think of G as $G := (X|Y = 0)$ and analogously $K := (X|Y = 1)$. Further, let g_1, \dots, g_{1000} and k_1, \dots, k_{10} be realization of G and K .

Then, random undersampling corresponds to randomly drawing an index set $I \subset \{1, 2, \dots, 1000\}$ with $|I| = 10$ and $\mathbb{P}(i \in I) = \frac{1}{1000}$ for $i = 1, \dots, 1000$. The resampled data set contains the collection of data points $\bigcup_{i \in I} \{g_i\}$ and $\bigcup_{i=1}^{10} \{k_i\}$. Conversely, random oversampling generates a data set consisting of $\bigcup_{i=1}^{1000} \{g_i\}$ and $\bigcup_{i=1}^{1000} \{k_{s_i}\}$, were s_i present random i.i.d. indices with $\mathbb{P}(s_i = j) = \frac{1}{10}$ for $j = 1, \dots, 10$.

Formally, we define resampling with the purpose of increasing the share of the minority class 1, without specifying the specific target ratio of minority and majority class, as follows.

Definition 1. Let $\mathcal{D} = \{(x_i, y_i)\}_{i=1}^N$ be i.i.d. samples generated from (X, Y) , where $Y|(X = x) \sim \text{Ber}(p(1|x))$. Let the data be imbalanced with minority class $Y = 1$, such that $\sum_i y_i < \sum_i (1 - y_i)$. We then call S a *resampling scheme*, if it generates data $\mathcal{D}^S = \{(x_i^S, y_i^S)\}_{i=1}^{N^S} \subset \mathcal{D}$ with $N^S > N$, respectively $N^S < N$, for which

$$\sum_{0 \leq i \leq N} (1 - y_i) = \sum_{0 \leq i \leq N^S} (1 - y_i^S) \quad \text{and} \quad \{(x_i, y_i) \in \mathcal{D} : y_i = 0\} \subset \mathcal{D}^S, \quad (\text{oversampling})$$

respectively

$$\sum_{0 \leq i \leq N} y_i = \sum_{0 \leq i \leq N^S} y_i^S \quad \text{and} \quad \{(x_i, y_i) \in \mathcal{D} : y_i = 1\} \subset \mathcal{D}^S \quad (\text{undersampling})$$

hold.

To indicate that we refer to empirical data, we write $\hat{p}(\cdot)$, $\hat{p}(\cdot, \cdot)$ and $\hat{p}(\cdot | \cdot)$ for the densities induced by the original data $\{(x_i, y_i)\}_{i=1}^N$. Reversely, $\hat{p}^S(\cdot)$, $\hat{p}^S(\cdot, \cdot)$ and $\hat{p}^S(\cdot | \cdot)$ are derived from resampled data $\{(x_i^S, y_i^S)\}_{i=1}^{N^S}$. Next, we impose that any proper resampling scheme should not alter the distribution of features in a given class, which is natural as any estimator $\hat{p} : x \mapsto \hat{p}(1|x)$ relies on features x .

Definition 2 (Consistent resampling). We call a resampling scheme S consistent if it preserves the observed probabilities for features X within every class $Y = y$, i.e. with $y \in \{0, 1\}$ fixed

$$\hat{p}^S(x|y) = \hat{p}(x|y)$$

holds for arbitrary $x \in X(\Omega)$.

Remark 1 (Examples for consistent resampling). Random undersampling and oversampling, as well as the popular resampling algorithm SMOTE, see [10], are all natural approaches to building a consistent resampling method. All approaches alter data x only for either the minority or the majority class. We provide arguments for the consistency of these resampling techniques, focusing on the class altered by the specific algorithm.

1. In random undersampling, we iteratively and randomly drop observation $(x, 0) \in \{(x_i, y_i)\}_{i=1}^N$. In the first iteration, the probability to drop $(x, 0)$ is characterized by the share of observations $x_i = x$ in class $y = 0$, which poses an estimator $\hat{p}(x|y = 0)$. Assuming a sufficiently large sample size for the majority class, i.e. $y = 0$, we can approximate the probability of subsequent observations $(x', 0)$ to be dropped by $\hat{p}(x'|y = 0)$.
2. In random oversampling, we iteratively draw observations $(x, 1) \in \{(x_i, y_i)\}_{i=1}^N$ with replacement. Hence, each x is drawn with probability $\hat{p}(x|y = 1)$.
3. SMOTE oversampling, see [10], also draws observations $(x, 1) \in \{(x_i, y_i)\}_{i=1}^N$ with replacement and with probability $\hat{p}(x|y = 1)$. In contrast to random oversampling, it does not sample x but $x' = x + u \cdot \tilde{x}$, where $u \sim U(0, 1)$ and \tilde{x} with $(\tilde{x}, 1) \in \{(x_i, y_i)\}_{i=1}^N$ a randomly chosen, k -nearest-neighbour to x . By default, SMOTE employs $k = 5$. This approach samples new data points by assuming $\hat{p}(x|y = 1)$ to be locally constant. The notion of locality is dictated by the distance metric used in the k -nearest neighbour algorithm.

According to the work in [17], the effect of consistent resampling can be formalized as follows.

Theorem 1 (Probabilistic view on resampling, see [17]). Let S be a consistent resampling scheme and (x, y) arbitrary data which satisfy $\hat{p}(x) > 0$ and $\hat{p}^S(x) > 0$. Then the equation

$$\hat{p}^S(1|x) = \hat{p}(1|x) \frac{\hat{p}^S(y = 1) (1 - \hat{p}(y = 1))}{\hat{p}(y = 1) (1 - \hat{p}(1|x)) + \hat{p}^S(y = 1) (\hat{p}(1|x) - \hat{p}(y = 1))}$$

holds.

In Theorem 1, the assumption of positives densities $\hat{p}(x) > 0$ and $\hat{p}^S(x) > 0$ is crucial to apply Bayes' rule $p(1|x) = p(x|1) p(y = 1) p(x)^{-1}$ in the proof of Theorem 1 for both \hat{p} and \hat{p}^S . In the simplest case, where estimators \hat{p} and \hat{p}^S are based on relative frequencies this certainly holds true for data (x, y) that are in the original and the resampled dataset. Next, we discuss the assumption of Theorem 1 for common classifiers.

Generalized linear models, tree based classifiers or neural networks all can be used to construct confidence predictions $\hat{p}(1|x)$ which are, at the very least, locally continuous. For example, a logistic regression or a neural networks with a final sigmoid activation both result in \mathbb{P} -almost-surely differentiable $\hat{p}(1|x) \in (0, 1)$ for all contracts x and, thus, $p(x) > 0$, see (10). In its standard form, see [26], classification trees apply relative frequencies per node, i.e. a locally constant estimator $\hat{p}(1|x)$. In pure nodes, where $\hat{p}(1|x) \in \{0, 1\}$, we find $p(x, y) = 0$ and $p(x) > 0$, see again (10).

Hence, the stated models all assume $p(x) > 0$ globally and show the generality of Theorem 1 in practice.

Observe that for any resampling schemes as in Definition 1 holds $\frac{1}{N^S} \sum_{y_i^S} y_i^S > \frac{1}{N} \sum_{y_i} y_i$. Hence, it is natural to assume that $\hat{p}^S(y=1) > \hat{p}(y=1)$ holds for modeling approaches in practice. Then, we can establish the effect of resampling from a distributional perspective.

Lemma 1 (Bias of traditional resampling). Let S be a consistent resampling scheme. Further, consider a modeling approach with $\hat{p}^S(y=1) > \hat{p}(y=1)$ and arbitrary data (x, y) with $\hat{p}(x) > 0$ and $\hat{p}^S(x) > 0$. Then, S increases the conditional distribution of the minority class 1, such that $\hat{p}^S(1|x) > \hat{p}(1|x)$ holds.

Proof. See Appendix A.1.

Following the standard rules of differentiation we can further analyse the bias indicated by Lemma 1.

Lemma 2. Let S be a consistent resampling scheme and (x, y) arbitrary data with $\hat{p}(x) > 0$ and $\hat{p}^S(x) > 0$. Then

$$\frac{\partial \hat{p}^S(1|x)}{\partial \hat{p}(1|x)} > 0 \quad \text{and} \quad \frac{\partial^2 \hat{p}^S(1|x)}{\partial \hat{p}(1|x)^2} < 0$$

holds.

Lemma 1 immediately implies that if $\hat{p}(1|x)$ is a consistent estimator, i.e. it \mathbb{P} -almost-surely converges to the true, latent probability $p(1|x)$ as the sample size $N \rightarrow \infty$, then $\hat{p}^S(1|x)$ formed on resampled data will not be consistent. In particular, if we look at Theorem 1 as a function of $\hat{p}(1|x)$ we can explicitly retrieve the relative bias introduced by resampling. As recorded in Lemma 2, resampling in particular alters low probabilities $\hat{p}(1|x)$ and results, if plotted against the non-resampling classifier \hat{p} , in a concave curve strictly above the line defined by the identity $\hat{p}^S(1|x) = \hat{p}(1|x)$.

Let us assume $\hat{p}(1|x)$ to be consistent. In the special case of perfectly balanced data, i.e. $\hat{p}^S(y=1) = \frac{1}{2}$, with an original base rate $\hat{p}(y=1)$ and the confidence predictions $\hat{p}^S(1|x)$, we can then explicitly reconstruct unbiased confidence predictions by

$$\hat{p}(1|x) = \hat{p}(y=1) \left(\hat{p}(y=1) + \frac{(1 - \hat{p}^S(1|x))(1 - \hat{p}(y=1))}{\hat{p}^S(1|x)} \right)^{-1}. \quad (11)$$

We conclude this section with remarks on resampling.

Remark 2.

- i) In a rare event setting the event probability $p(1|x)$ is generally low, leading to a small region in the feature space $X(\Omega)$ to be classified as the minority event. Lemma 1 and 2 illustrate that resampling increases this region and, thus, allows to shift the decision boundary of a classifier. For label predictions, this has empirically been shown to improve frequentistic metrics, see [10, 51].
- ii) If the given data represents the ground truth in the sense that data $\{(x_i, y_i)\}_{i=1}^N$ are i.i.d. realizations from (X, Y) that allow for a sound estimation, in the sense of $\mathbb{E}_{x \sim X} [p(1|x) - \hat{p}(1|x)] = 0$, then resampling introduces a bias to our confidence predictions $\hat{p}^S(y|x)$. In particular, any risk measure, as e.g. the value-at-risk, applied to the distribution induced by $\hat{p}^S(y|x)$ will reflect this bias.
- iii) It is obvious that random-undersampling disregards most of the information contained in data of the majority class. A natural approach to mitigate the loss of information is to use bootstrapping to obtain multiple balanced, random-undersampled training data and apply ensemble techniques, which have shown superior performance e.g. in [49].

5 Data

There exists a large number of empirical work that aims to describe the nature of the surrender probability $p(1|x)$, where x includes macroeconomic, microeconomic and contractual factors, see [2, 7, 15, 29, 41, 52]. As the nature of $p(1|x)$ seems to vary between countries and types of policy, we do not aim to construct an optimal estimator $\hat{p}(1|x)$ for all life insurance business. Our experiments focus on endowment contracts only. Further, we look at individual findings of the literature to construct four latent surrender models p of varying nature and complexity, which we call *surrender profiles*. Then, for each surrender profile we estimate p with a particular focus on the consistency of estimator \hat{p} and the effect of resampling. In the following, we summarize how data $\{(x_i, y_i)\}_{i=1}^N \sim (X, Y)$ is generated.

Simulation of contracts x . Each endowment contract $x_i = (x_i^{(1)}, \dots, x_i^{(n)})$ is identified by the current age of the policyholder, the face amount, the duration of the contract, the elapsed duration, the remaining duration, the annual premium amount, the frequency of premium payments and the current calendar year. We start by generating a portfolio of $N = 30'000$ endowment contracts at calendar year 0, where we infer a realistic distributions of X from [40]. In [40], the authors provide detailed statistics on a portfolio of US whole life contracts. Given the similarity between endowment and whole life insurance¹, the portfolio in [40] provides a realistic basis for our experiments. In Figure 1 we provide an illustration of the marginal distributions of the portfolio at calendar year 0. Face amounts are calibrated such that annual premiums are consistent with [40]. To compute premiums we apply the equivalence-principle, see [13, 21], under the following assumptions.

- The actuarial interest rate i is constant with $i = 0.02$.
- Expenses of the insurer for acquisition, administration and amortization of each contract are represented by $(\alpha, \beta, \alpha^\gamma) = (0.025, 0.03, 0.001)$, see [7].
- Premiums are paid up to the age of 67, the German age of retirement². Up-front premium payments are annualized linearly by the remaining time of premium payments.
- Mortality is described by a parametric survival model based on the Makeham Law, see [13]. The t -year survival probability tp_a of individual aged a is defined by

$$tp_a := \exp \left(-At - \frac{B}{\log(c)} c^a (c^t - 1) \right), \quad (12)$$

where we adopt the parameters of [13] by setting the baseline hazard $A = 0.00022$ and age related factors $B = 2.7 \cdot 10^{-7}$ and $c = 1.124$.

More detail on the simulation of data at calendar year 0 can be found in the Appendix A.2. All contracts are then iterated forward by increasing the age of the policyholder and the elapsed duration of the contract by the period length

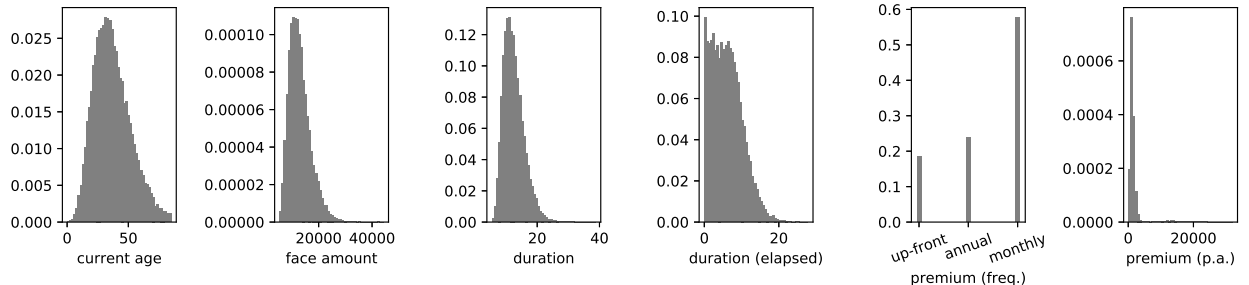


Figure 1: Marginal distribution of the portfolio at calendar year 0.

¹A whole life insurance is equivalent to an endowment insurance with infinite duration.

²To be precise, the age of retirement in Germany varies between 65 and 67 based on the date of birth. The basic retirement at 67 applies for individuals born on 1 January 1964 or later, see [35].

of one year. All other features are assumed to remain constant, i.e. changes to policies are not admissible. Additionally, at every iteration we simulate new business at the magnitude of 6% of the existing business, which was empirically observed in the German market, see [23]. Contracts of the new business are simulated analogously to the portfolio at calendar year 0, naturally with the restriction that the elapsed duration equals zero. The time frame of our data is set to 15 one-year periods.

Meta model $p(1|\cdot)$. Given the input variable $x = (x^{(1)}, \dots, x^{(n)})$, we use a logistic regression model to obtain the true surrender probability $p(1|x)$ by

$$p(1|x) := \left(1 + \exp(-\beta_0 - \beta_x' x)\right)^{-1}, \quad (13)$$

where the regression coefficients $\beta_0 \in \mathbb{R}$ and $\beta_x : \mathbb{R}^n \rightarrow \mathbb{R}^n$ are specified by the respective surrender profile. In contrast to its standard formulation, see [26], we denote coefficients β_x as a function of x . We do so purely for notational convenience, as it allows us to set the effect $\beta_x^{(i)} x^{(i)}$ of the i th feature as piecewise constant without having to introduce hot-encoded auxiliary variables. This will be useful when describing our surrender profiles. Additionally, we note that the use of categorized risk drivers increases the complexity of the model $p(1|x)$, which is in line with the complexity of surrender activities.

In [8, 15, 41], the authors report specific values of $\beta_x^{(i)} x^{(i)}$ for a variety of categorized risk drivers $x^{(i)}$. We adopt and combine these values in four different surrender profiles, see Figure 2 for an illustration. We consider the current age of a policyholder, the duration elapsed since underwriting the contract, the maximum duration of the contract, as well as the remaining duration until maturity, the frequency of premium payments and the annualized premium amount. In surrender profile 4, the most complex setting, we additionally include a time factor represented by calendar years, which can be interpreted as a proxy of the economic environment at that time or alternatively as noise. The range of profiles covers a variety of plausible dynamics, for example elevated surrender of young or higher ages, increased surrender at an early stage of contracts, for short-term contracts in general or higher surrender for higher amounts of annual premiums. The intercept β_0 of each profile has been adjusted, such that observed surrender rates per calendar year fall into realistic ranges of 0.01 up to 0.05. In the Appendix A.3 we provide additional detail on the formulation of all surrender profiles.

Simulation of surrender activity y . We observe a contract x only up to its termination T , in our case either maturity, death or surrender. Maturity events are easily identified by the duration of a contract, unless death or surrender occurs prior. To simulate the death of a policyholder with current age a we numerically invert tp_a as a function of t and obtain the time of termination by $T = (tp_a)^{-1}(u)$, $u \sim \mathcal{U}(0, 1)$. Naturally, we do so only once per policyholder. More detail on inverse transform sampling can be found in [24]. Surrender events are computed iteratively. A policyholder with contract x realizes a surrender event $y = 1$ within the next year if and only if $p(1|x) \geq v$ for $v \sim \mathcal{U}(0, 1)$. If surrender and an alternative termination event are modeled to occur in the same year, we assume uniformity of the events, similar to fractional survival probabilities in [21]. Given time $t \in (0, 1)$ until the alternative termination event occurs, we assume that the surrender event occurs with probability t prior to the competing risk, i.e. maturity or death.

Data preparation. We one-hot encode the categorical feature 'frequency of premium payments' and apply min-max scaling to scale all contracts x to the range of $[0, 1]^n$. For the sake of readability, both the raw and the scaled contract by x . Next, we split our data $\{(x_i, y_i)\}_{i=1}^N$ in time at the calendar year at which at least 70% of data has been observed. Depending on the specific surrender profile, this split occurs at calendar years $t \in \{8, 9\}$ and results in training data $\mathcal{D}_{\text{train}}$ and test data $\mathcal{D}_{\text{test}}$. Note that a split in time imitates a practical setting, where we test the model from a going concern perspective. A random train-test split would result in training on future data. Moreover, a split in time enables us to detect a potential bias of our model as the decomposition of the portfolio changes. Although we model new business to follow a stationary distribution, respectively all features but elapsed duration and the current calendar year, the inclusion old business causes the composition of the portfolio to be non-stationary, e.g. with an increasing share of older policyholders or older contracts. Last, we randomly set aside 30% of the training data for validation.

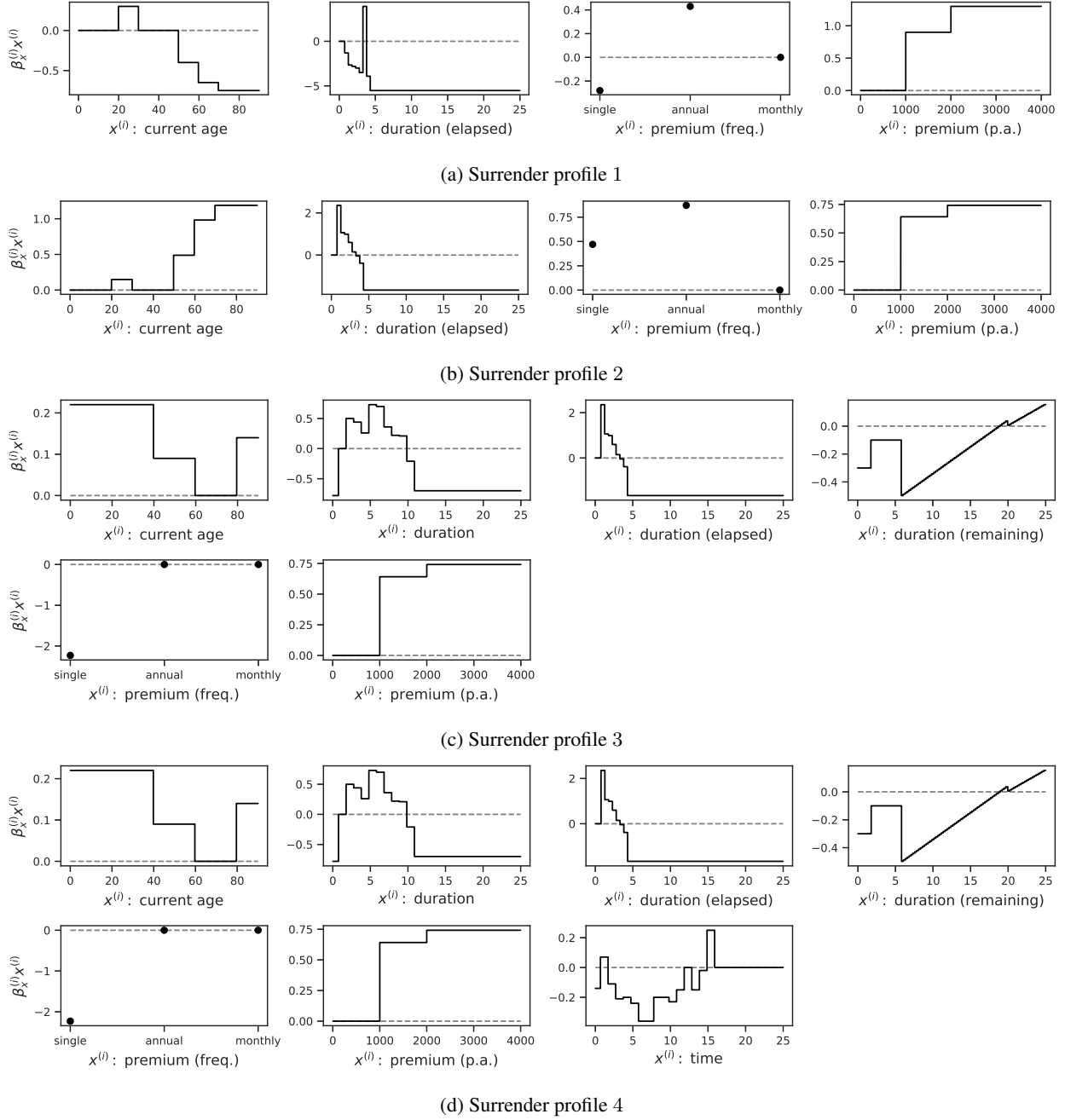


Figure 2: Collection of distinct surrender profiles in our experiments.

In the Appendix A.5, see Table 4, we additionally provide a summary of the number of one-year observations in training and test set, the imbalance of surrender and non-surrender events and the size of the training data set after random-undersampling or SMOTE-resampling to perfect balance. Without resampling, surrender events contribute a share of 0.01 up to 0.045 of all observations, which highlights the rare event character of our setting.

6 Numerical experiments

We present results for modeling $p(1|x)$, given the four different surrender profiles and data $\{(x_i, y_i)\}_{i=1}^N$ discussed in Section 5. We apply three model types, the logistic regression, tree based classifiers and neural networks, in their bagged and boosted form. As a substitute for a thorough exploratory data analysis, for each surrender profile we restrict the input to its estimator $\hat{p}(1|x)$ to the components of x_i that actually are part of the latent surrender model $p(1|x)$. Let us briefly comment on the specifics of the estimators.

Baseline model. To set a baseline, we introduce a classifier with a constant surrender rate. Due to its simplicity, this provides a practical supervision whether subsequent classifiers are plausible and whether their increasing complexity is justified. Given a set of training data $\mathcal{D}_{\text{train}}$, which differ for each surrender profile, we define the confidence prediction \hat{p} of the baseline model by

$$\hat{p}(1|x') \equiv \frac{1}{|\mathcal{D}_{\text{train}}|} \sum_{(x,y) \in \mathcal{D}_{\text{train}}} y ,$$

where x' presents an arbitrary contract.

Logistic regression. The structure of the logistic regression is given by $p(1|x) := (1 + \exp(-\beta_0 - \beta' x))^{-1}$, with intercept $\beta_0 \in \mathbb{R}$ and coefficients $\beta \in \mathbb{R}^p$. Note that in contrast to the meta model $p(1|x)$, coefficients β are constants. Providing the estimator with the true categories of all components of x , e.g. indicating ages 20-30 to be highly susceptible to surrender, seems unrealistic in a practical rare event setting. Instead, we feature engineer higher degree inputs $(x_i^{(j)})^k$ for each feature $x_i^{(j)}$ and $k = 1, \dots, 10$, as long the binary-crossentropy on the validation set decreases. More detail on greedy forward-stepwise selection can be found in [26]. Note that the surrender profiles do not consider interactions between features, which is why we do not engineer inputs of the form $(x_i^{(l)})^k (x_i^{(n)})^m$. To avoid overfitting, we additionally apply the L_2 -regularization $\sum_{i>0} (\beta^{(i)})^2$ when minimizing the cross-entropy loss. At last, we combine $N_{\text{bag}} = 10$ estimators to an ensemble model³, since a single logistic estimator is highly volatile in a rare event setting, see again [26].

Tree based classifiers. A tree based classifier provides a split of the feature space $X(\Omega)$ into disjoint regions R_1, \dots, R_m . The surrender probability $\hat{p}(1|x)$ is then formed by relative frequencies per regions R_k . For an arbitrary data point $x' \in R_k$ we look at the subset $\mathcal{D}_{R_k} = \{(x, y) \in \mathcal{D}_{\text{train}} : x \in R_k\}$ and assign

$$\hat{p}(1|x') = \frac{1}{|\mathcal{D}_{R_k}|} \sum_{(x,y) \in \mathcal{D}_{R_k}} y .$$

For an individual classification and regression tree (CART), see [26], regions R_k are the result of recursive, binary splits of the region $X(\Omega)$. At each recursion, a CART searches for the feature $x^{(i)}$ and the hyperplane $H := \{x : x^{(i)} = c\}$, $c \in \mathbb{R}$, such that the respective split by H leads to a maximum reduction of the impurity. We measure the impurity of a region R by the binary cross-entropy⁴. To avoid overfitting, we perform a best parameter search for the maximum depth T of a single CART based on the cross-entropy loss on the validation set and eventually set $T = 5$, i.e. allowing for 2⁵ binary splits. Finally, we use ensemble techniques and form a random forest classifier with $N_{\text{bag}} = 100$ trees as in [26] and a gradient boosting decision tree with $N_{\text{boost}} = 100$ trees, the XGBoost classifier as in [11]. Both ensemble techniques utilize uniform bootstrapping with a fixed sample size $|\mathcal{D}_{\text{train}}|$, leading to varying training data for every CART.

Remark 3. In practice, a more recent gradient boosting decision trees as LightGBM, which is designed for high-dimensional features spaces and large data sets, see [22], might be beneficial. In our experiments with a low-dimensional feature space, we observe a speed up of LGBoost compared to an already fast XGBoost model, but no improvement in model performance.

³For completeness, we also tested adaptive boosting as in [45] on polynomial features, but dropped it due to poor performance.

⁴We note that the alternative *Gini index*, see [26], yielded comparable results in our experiments.

Neural network classifiers. The bagged model consists of neural networks $\hat{p}^{(k)}(1|\cdot)$, which are trained independently for $k = 1, \dots, N_{\text{bag}}$ with $N_{\text{bag}} = 5$. All models $\hat{p}^{(k)}$ have the same architecture. We choose feed-forward networks with 3 hidden layers of decreasing widths of 30, 20 and 10 with two ReLu and a tanh activation function. The output layer has a single unit and a sigmoid activation σ . The bagged estimator is then formed by $\hat{p}(1|x) := \frac{1}{N_{\text{bag}}} \sum_k \hat{p}^{(k)}(1|x)$. Each sub-model $\hat{p}^{(k)}$ consists of $30(n+1) + 871$ parameters. Note that the feature 'premium frequency' is one-hot-encoded, resulting in effectively $n+1$ inputs to the neural network.

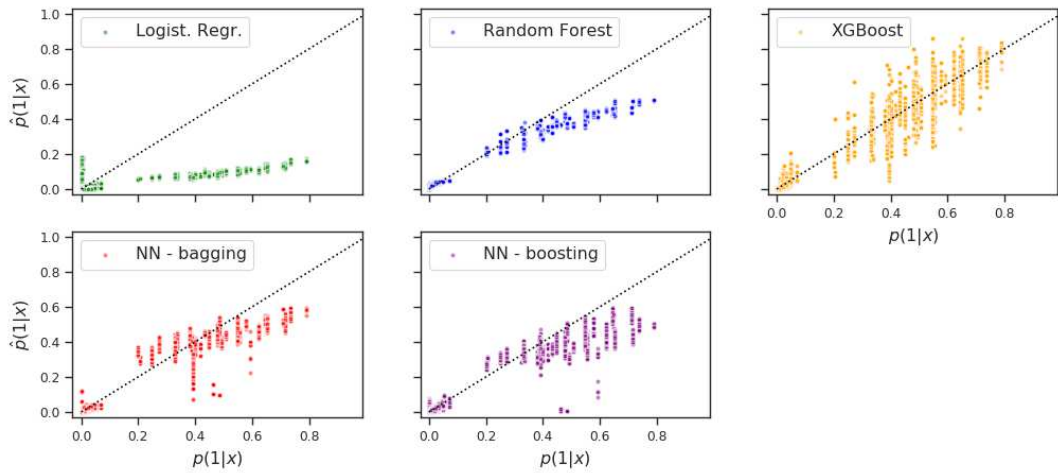
Additionally, we construct a boosted neural network. Motivated by experiments and [3], we choose shallow neural networks $p^{(k)}$, $k = 1, \dots, N_{\text{boost}}$ as weak learners with $N_{\text{boost}} = 20$. For $k > 1$, each network $p^{(k)}$ has one hidden layer with 10 units for each input feature in the respective surrender profile, a ReLu activation in the hidden layer and a single output unit with a linear activation. Hence, each weak learner $\hat{p}^{(k)}$, $k > 1$, consists of $(n+3)10n+1$ parameters. We start the boosting procedure with the baseline rate of $\hat{p}^{(1)}(1|x) := \sigma^{-1} \left(\frac{1}{|\mathcal{D}_{\text{train}}|} \sum_i y_i \right)$ for training data $(x_i, y_i) \in \mathcal{D}_{\text{train}}$. We then iteratively add and interdependently train weak learners $p^{(k)}$ until we obtain the final boosted model $\hat{p} : \mathbb{R}^p \rightarrow (0, 1)$ by

$$\hat{p}(1|x) := \sigma \left(\sum_{k=1}^{N_{\text{boost}}} \hat{p}^{(k)}(1|x) \right). \quad (14)$$

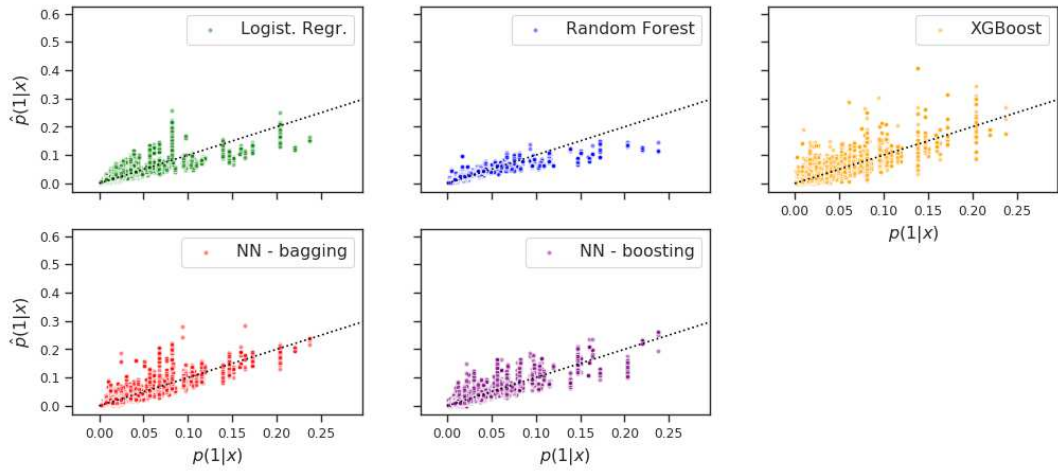
All neural networks are trained with stochastic gradient descent on the cross-entropy loss, implemented by the adam algorithm, see [31], using a batch size of 1'024 and a maximum of 2'000 epochs. To mitigate overfitting, we apply early stopping if the validation loss does not decrease for 25 epochs. For the bagged estimator, in addition to training $\hat{p}^{(k)}$ individually, we perform a final fine tuning where we train $\hat{p}(1|x)$ collectively, as done e.g. in [28]. For the boosted estimator, we include a corrective step after iteration $i \in \{5, 10, 15, 20\}$, in which we collectively fine tune the model $\sigma \left(\sum_{k \leq i} \hat{p}^{(k)} \right)$, see [3]. Note that in contrast to [3], that utilizes gradient boosting and hence a Taylor approximation, we work with the exact cross-entropy loss. While this is computationally more expensive as we do not train on residuals, it allows us to use the sigmoid function σ in (14) to ensure sound confidence predictions $\hat{p}(1|x) \in (0, 1)$.

Numerical results. Let us now evaluate the classifiers mentioned above for all four surrender profiles. We start with a hypothetical analysis, where we assume that we can access the true probability of surrender within the next year of arbitrary contract x . While this quantity $p(1|x)$ is not available in practice it yet provides instructive insight into the classifiers performance and allows us to compare the bias of resampling to Lemma 1 and 2 numerically. We start with a qualitative analysis of bias and variance of the models before we provide statistics to quantify our observations and the effect of resampling. Lastly, we look at the modelled mean surrender rate over calendar-time, including confidence bands, for all classifiers and all profiles. In summary, we will see XGBoost to be the superior model, closely followed by neural classifiers, and confirm the bias of resampling numerically. Additionally, we will notice that model evaluation by a single value, e.g. cross-entropy, is insufficient as it ignores the non-stationarity of our data. Further, mean surrender rates with confidence bands as in Corollary 1 will provide a more comprehensive perspective.

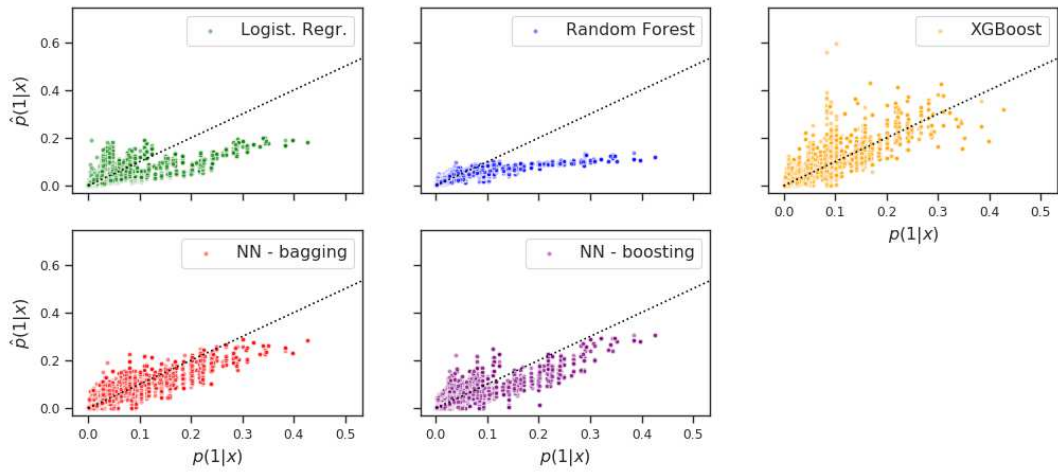
In Figure 3 we consider test data $(x, y) \in \mathcal{D}_{\text{test}}$ and plot the label predictions $\hat{p}(1|x)$ against the true, latent surrender probability $p(1|x)$ for all discussed models and all four surrender profiles. We observe that XGBoost is the only classifier that is approximately unbiased for all surrender profiles, yet its prediction $\hat{p}(1|x)$ exhibit a comparably high variance. In contrast, predictions of the random forest and the bagged logistic classifier indicate a lower variance, but consistently underestimate the lapse probability of contracts x that posses a comparably high risk of surrender. Recall that two lapse events \hat{y}_1, \hat{y}_2 are realizations of different random variables $(Y|X = x)$, given the underlying contracts x_i, x_j do not coincide. Hence, this bias refers to a specific type of high-risk contracts, but not the tail of a single distribution. Lastly, both neural network approaches show a slight bias towards underestimating the lapse probability of high-risk contracts (profile 1 and 3), see Figures 3a and 3c, with less variance in $\hat{p}(1|x)$ than XGBoost. For risk profile 2, see Figure 3b, both neural networks suggest a performance superior to XGBoost, as they are approximately



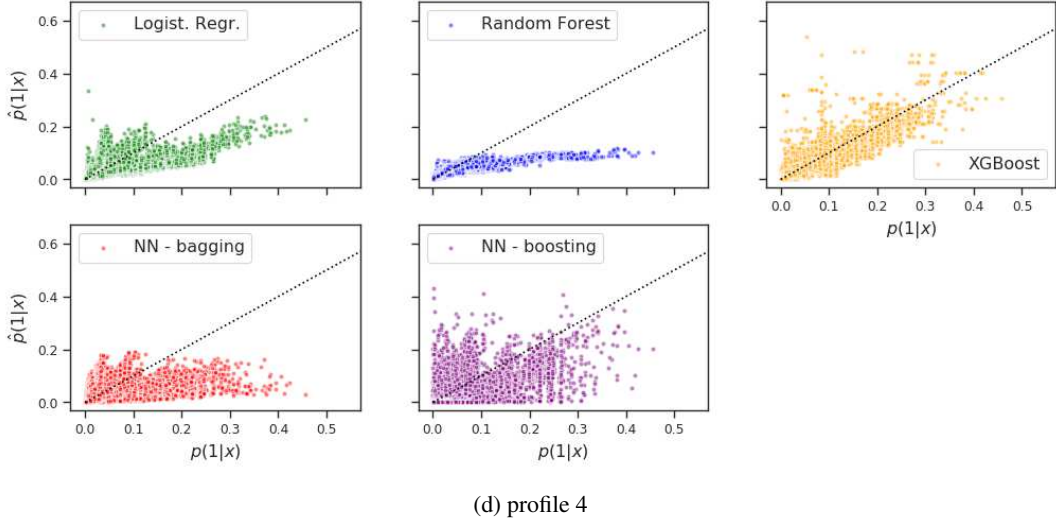
(a) profile 1



(b) profile 2



(c) profile 3



(d) profile 4

Figure 3: p - \hat{p} plots of the discussed classifiers for surrender profiles 1-4.

unbiased with lower variance. In profile 4, the bagged network consistently underestimates the surrender probability of contracts with comparably high surrender risk and the boosted estimator provides a classifier with high variance. Recall that in profile 4 we add non-stationary noise with regard to the calendar year, see Appendix A.3. While it might initially seem like our neural network approaches are overfitting on the training data in profile 4, we note that profile 4 is particularly challenging as observations on the input feature 'calendar year' are different in training and test data. Moreover, the effect of the calendar year t on surrender is increasingly negative in the training data, whereas the reverse holds for the test data, see Figure 2d. This setting forces classifiers to extrapolate the effect of the calendar year. While this adverse effect might be mitigated by selecting the validation data \mathcal{D}_{val} also with respect to calendar time, instead of randomly, we take this use-case to eventually highlight the benefit of a probabilistic evaluation. Recall that the illustrated p - \hat{p} plot cannot be used for tuning hyperparameters, as the true probabilities $p(1|x)$ are unknown.

Next, we quantify our observations in Table 1, where we provide latent quantities, as the mean value $\text{mae}(p, \hat{p})$ (in short: mae) and the variance (Var) of the errors $|p(1|x) - \hat{p}(1|x)|$, but also observable quantities as the accuracy, the F_1 -score and the binary cross-entropy. All results are provided for training and test data separately. In each column we highlight the best value. Note that computing the variance of the errors $|p(1|x) - \hat{p}(1|x)|$ is fundamentally different from computing the variance of label predictions $\hat{p}(1|x)$. While the later is observable and gives the intuition that e.g. the logistic regression in Figure 3a has little variance, it disregards the fact that every contract x induces an individual random variable $(Y|X = x)$, which is to be modeled by $\hat{p}(1|x)$. Hence, the variance of predictions $\hat{p}(1|x)$ holds little value as it penalizes e.g. an unbiased classifier if true probabilities $p(1|x)$ evenly populate $[0, 1]$.

For profiles 1 and 4, see Tables 1a and 1d, XGBoost shows the lowest variance and mean absolute error on both train and test data. The low variance of latent errors $|p(1|x) - \hat{p}(1|x)|$ is in contrast to the comparably high variance of observable predictions $\hat{p}(1|x)$. For profiles 2 and 3, see Tables 1b and 1c, neural classifiers perform equally well as XGBoost, respectively even slightly outperform it. The other classifiers, bagged logistic regression and random forest, also show improvements in mean absolute error and variance over the naive baseline. Depending on the desired bias-variance trade-off, one can even argue the logistic regression to be the best choice for profile 2. Overall, in each profile the best classifier improves the mean absolute error by about 1%, with the exception of profile 1 where the absolute improvement is as high as 4.6%. Later in this section, when we take a time series perspective to examine observed surrender rates per calendar year, we will observe that simply adding a constant risk buffer of e.g. 0.01 to our baseline model is not sufficient to cover our exposure to surrender risk. For now, let us look at the actually observable evaluation metrics in Table 1. We notice that the binary cross-entropy (in short: entropy) and the latent mean absolute

Data Evaluation	Train.					Test				
	acc.	F_1	entropy	mae	Var	acc.	F_1	entropy	mae	Var
Baseline	0.9710	0.0000	0.1311	0.0495	0.0101	0.9546	0.0000	0.1890	0.0641	0.0158
Logist. Regr.	0.9710	0.0000	0.1008	0.0445	0.0084	0.9546	0.0000	0.1352	0.0520	0.0128
Random Forest	0.9732	0.2003	0.0532	0.0120	0.0007	0.9558	0.0867	0.0770	0.0154	0.0010
XGBoost	0.9818	0.6866	0.0429	0.0058	0.0006	0.9628	0.5934	0.0719	0.0080	0.0008
NN - bagging	0.9739	0.4440	0.0532	0.0090	0.0014	0.9581	0.2479	0.0733	0.0088	0.0009
NN - boosting	0.9732	0.3780	0.0607	0.0156	0.0025	0.9571	0.1823	0.0765	0.0118	0.0013

(a) profile 1

Data Evaluation	Train.					Test				
	acc.	F_1	entropy	mae	Var	acc.	F_1	entropy	mae	Var
Baseline	0.9835	0.0000	0.0842	0.0199	0.0011	0.9869	0.0	0.0703	0.0200	0.0011
Logist. Regr.	0.9835	0.0000	0.0721	0.0110	0.0006	0.9869	0.0	0.0614	0.0106	0.0006
Random Forest	0.9835	0.0000	0.0704	0.0119	0.0008	0.9869	0.0	0.0608	0.0122	0.0009
XGBoost	0.9838	0.0485	0.0631	0.0117	0.0010	0.9869	0.0	0.0610	0.0125	0.0011
NN - bagging	0.9835	0.0000	0.0713	0.0105	0.0007	0.9869	0.0	0.0609	0.0104	0.0007
NN - boosting	0.9835	0.0000	0.0717	0.0116	0.0009	0.9869	0.0	0.0608	0.0115	0.0009

(b) profile 2

Data Evaluation	Train.					Test				
	acc.	F_1	entropy	mae	Var	acc.	F_1	entropy	mae	Var
Baseline	0.9799	0.0000	0.0984	0.0254	0.0016	0.9838	0.0	0.0831	0.0242	0.0013
Logist. Regr.	0.9799	0.0000	0.0865	0.0205	0.0012	0.9838	0.0	0.0728	0.0187	0.0011
Random Forest	0.9799	0.0000	0.0835	0.0172	0.0011	0.9838	0.0	0.0710	0.0162	0.0010
XGBoost	0.9801	0.0181	0.0724	0.0140	0.0010	0.9838	0.0	0.0689	0.0141	0.0011
NN - bagging	0.9799	0.0009	0.0806	0.0148	0.0010	0.9838	0.0	0.0693	0.0141	0.0010
NN - boosting	0.9799	0.0018	0.0819	0.0158	0.0010	0.9838	0.0	0.0710	0.0147	0.0010

(c) profile 3

Data Evaluation	Train.					Test				
	acc.	F_1	entropy	mae	Var	acc.	F_1	entropy	mae	Var
Baseline	0.9790	0.0000	0.1017	0.0219	0.0011	0.9841	0.0	0.0823	0.0190	0.0007
Logist. Regr.	0.9790	0.0000	0.0890	0.0173	0.0008	0.9841	0.0	0.0720	0.0143	0.0005
Random Forest	0.9790	0.0000	0.0867	0.0136	0.0007	0.9841	0.0	0.0707	0.0108	0.0004
XGBoost	0.9792	0.0162	0.0742	0.0096	0.0005	0.9841	0.0	0.0679	0.0087	0.0003
NN - bagging	0.9790	0.0000	0.0843	0.0130	0.0007	0.9841	0.0	0.0740	0.0149	0.0007
NN - boosting	0.9791	0.0013	0.0849	0.0144	0.0007	0.9841	0.0	0.0829	0.0151	0.0007

(d) profile 4

Table 1: Statistics of the discussed classifiers for surrender profiles 1-4.

error are highly correlated, yet not perfectly aligned, see e.g. Table 1b. From a frequentistic perspective, for profiles 2-4 all classifiers yield the identical accuracy and F_1 -score on the test set. Since for these profiles the true surrender probability $p(1|x)$ does not exceed 0.5, recall Figure 3, which is the default threshold $c \in [0, 1]$ to obtain label predictions $\hat{y} = \mathbb{1}_{\{\hat{p}(1|x) \geq c\}}$, any sound classifier will show this behavior. As $p(1|x)$ is not accessible in practice and cannot be used for evaluation or to check for plausibility, we follow the common strategy of resampling to improve the F_1 -score.

We retrained all models discussed above on balanced data, altered by random-undersampling or SMOTE-resampling. As the quality of our results was equal regardless of the specific surrender profile or the type of resampling applied, we restrict our presentation to SMOTE-resampling on surrender profile 2. Profile 2 is arguably the hardest profile to form accurate label predictions on, as even on the training data all models except XGBoost showed a zero F_1 -score, see Table 1b.

In Table 2 we revisit the evaluation of our classifiers, which now have been trained on resampled data. We evaluate all classifiers on the actually observed training and test data. We notice that resampling indeed improves the F_1 -score of all classifiers on the training as well as the test data. This means that SMOTE-resampling positively affects the balance between correct label predictions $\hat{y} = 1$ and correctly classified observations $y = 1$. While this might be the objective in situations where binary actions have to be taken, e.g. the decision to investigate for fraud, Table 2 also shows its downside. First, there is a trade-off between F_1 -score and accuracy. Secondly and arguably more importantly, we

Data Evaluation	Train.					Test				
	acc.	F_1	entropy	mae	Var	acc.	F_1	entropy	mae	Var
Baseline	0.9835	0.0000	0.0842	0.0199	0.0011	0.9869	0.0000	0.0703	0.0200	0.0011
Logist. Regr.	0.7512	0.0922	0.5119	0.3245	0.0471	0.7714	0.0749	0.4850	0.3084	0.0451
Random Forest	0.7232	0.0874	0.4944	0.3252	0.0435	0.7530	0.0720	0.4551	0.3042	0.0398
XGBoost	0.8202	0.1185	0.4151	0.2653	0.0497	0.8723	0.0933	0.3038	0.2022	0.0377
NN - bagging	0.7640	0.0997	0.4549	0.2816	0.0596	0.7824	0.0754	0.4165	0.2581	0.0563
NN - boosting	0.7663	0.0985	0.4778	0.2944	0.0562	0.7829	0.0770	0.4489	0.2731	0.0552

Table 2: Statistics on the discussed classifiers with SMOTE-resampling for surrender profile 2.

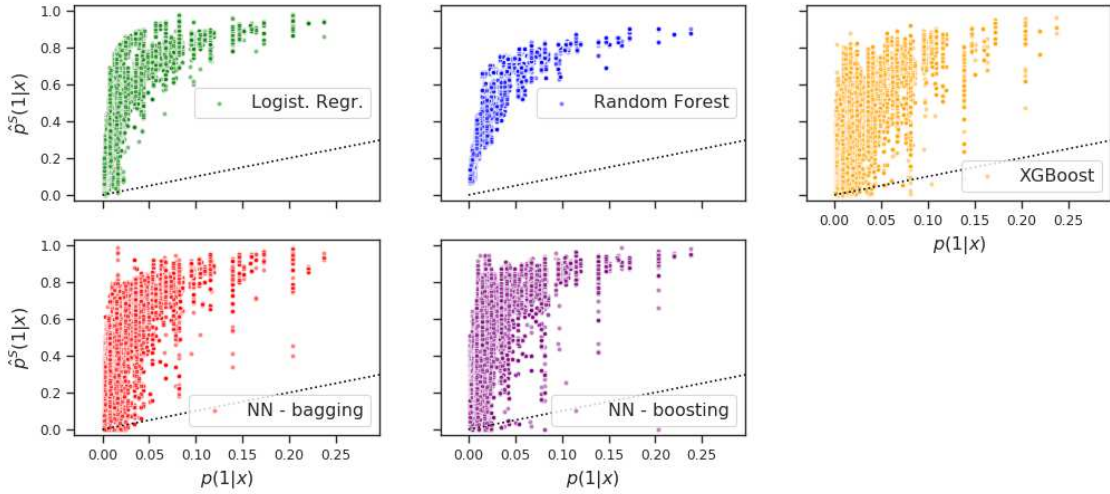


Figure 4: p - \hat{p}^S plots of the discussed classifiers and SMOTE-resampling for surrender profiles 2.

observe that the cross-entropy as well as the mean and variance of the latent errors $|p(1|x) - \hat{p}^S(1|x)|$ have increased for all classifiers on training and test data, compared to training without SMOTE-resampling, see Figure 1b. We can uncover the later even further by looking at p - \hat{p}^S -plots, see Figure 4. Here, we clearly observe that resampling (with SMOTE) results in confidence prediction $\hat{p}^S(1|x)$ that in general highly overestimate the true surrender probability $p(1|x)$ of contract $x \in \mathcal{D}_{\text{test}}$. Further, the quantities $\hat{p}^S(1|x)$ approximately form a concave curve with respect to the true probabilities $p(1|x)$. This numerically affirms Lemma 1 and 2. Note that both lemmata describe the relation between \hat{p} and \hat{p}^S , e.g. $\hat{p}^S(1|x) > \hat{p}(1|x)$, and that prior to resampling classifiers occasionally underestimate the true probability $p(1|x)$ by $\hat{p}(1|x)$, see again Figure 3b. Ignoring the numerical nature of training, this is why we naturally observe a few estimates $\hat{p}^S(1|x)$ below the line defined by the identity $\hat{p}^S = p$.

Remark 4. Alternatively, to improve the F_1 -score one might alter the threshold $c \in [0, 1]$ which label predictions $\hat{y} = \mathbb{1}_{\{\hat{p}(1|x) \geq c\}}$ are based on. For completeness, we also investigated ROC and precision-recall-curves. However, we found no significant benefit of resampling in terms of the classifiers' AUC-values, which is why we do not report results on this. Another downside of resampling, and oversampling in particular, is its more demanding run time. In our experiments, random undersampling and SMOTE-resampling lead to an increased run time of a factor up to 6.3, resp. 8.5, see Table 5 in Appendix A.5.

Remark 5. The bias of resampling schemes indicated by Figure 4 naturally leads to mean surrender rates $\frac{1}{|\mathcal{D}|} \sum_{(x,y) \in \mathcal{D}} \hat{p}^S(1|x)$ that highly and confidently overestimate the observed surrender rate $\frac{1}{|\mathcal{D}|} \sum_{(x,y) \in \mathcal{D}} y$ for data \mathcal{D} of a specific calendar year. If we were to work with label predictions, we could alternatively estimate mean surrender rates by relative frequencies $\frac{1}{|\mathcal{D}|} \sum_{(x,y) \in \mathcal{D}} \mathbb{1}_{\{\hat{p}(1|x) \geq c\}}$. However, in our experiments this led to performances unsuitable for application, as we still considerably overestimate the observed surrender rate. Also, binary label predictions prevent us from constructing confidence bands as described in Corollary 1.

At last, we omit resampling and evaluate all classifiers in a practical setting, where we cannot access the latent probabilities $p(1|x)$. We now take a time-series perspective and look at predicted mean surrender rates and their confidence bands over calendar-time, as proposed in Corollary 1. This concept uncovers the quality of the proposed classifiers in a going concern setting and respects that our insurance portfolio might change over time, leading to non-constant risk exposure e.g. in term of a value-at-risk measure. The results are illustrated in Figure 5, where the split in calendar time between train and test data is indicated by a vertical, gray line. Upper and lower $\alpha = 0.95$ confidence bands, as in Corollary 1, are displayed by up- respectively down-facing triangles.

First, we observe that the mean surrender rates are non-stationary. Profiles 2-4 show mean surrender rates that decline over time. In contrast, in profile 1 we see an increase of mean surrender activity with a notable drop at calendar year 4. Recall that surrender profile 1 as in [41] exhibits a significant increase in surrender activity just prior the an elapsed duration of 4 years, followed by a sharp decline.

For all surrender profiles, the naive baseline provides an insufficient classifier, which naturally does not capture any of the non-stationarity. Hence, a constant risk buffer does not appropriately compensate the simplicity of the model. In profile 1, we observe that all classifiers except the logistic regression capture the trend of mean surrender, including the characteristic, sharp drop at calendar year 4. However, XGBoost is the only classifier for which the true rate lies consistently within the confidence band of its predictions. In profiles 2 and 3, for most years the quality of the proposed classifiers, excluding the naive baseline, cannot be distinguished based on their 0.95-confidence bands. Arguably, random forest and logistic regression indicate a performance inferior to neural classifiers and XGBoost, which is again the only model that confidently predicts the true surrender rate for all calendar years. This is actually surprising, given that in profile 2 for both neural classifiers the mean error $|p(1|x) - \hat{p}(1|x)|$ is lower than for XGBoost, recall Table 1b. This highlights the importance of a calendar-year, respectively time series, perspective on surrender. In profile 4 we expect our neural classifiers to show poor performance, given that we forced them to extrapolate the feature 'calendar year', recall Figure 3d and its reasoning. However, this expectation is purely based on accessing the true surrender probability $p(1|x)$, which is latent in practice. In Figure 5d we now observe precisely this behaviour. The mean

surrender rates of both neural classifiers, as well as the logistic regression, drift away from the true surrender rate on the test set. Hence, predicted mean surrender rates and in particular their confidence bands successfully uncover the previously latent weakness of models. In that sense, results on profile 4 also indicate tree based classifiers to provide more stable estimates when characteristics of training and test set differ.

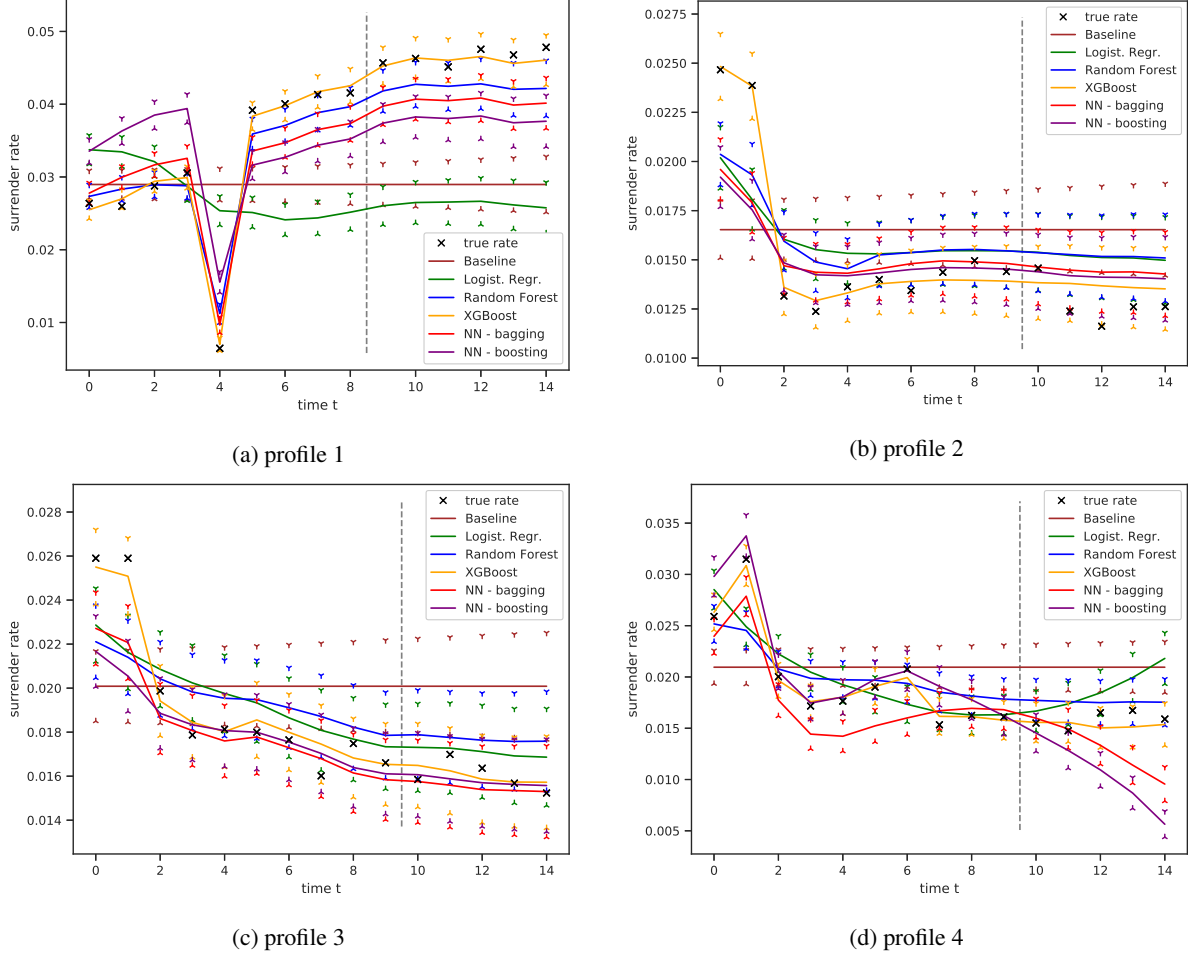


Figure 5: Mean surrender rates over calendar-time of the classifiers for surrender profiles 1-4, including confidence bands ($\alpha = 0.95$) based on Corollary 1. Vertical lines indicate a train-test-split.

7 Conclusion

In the present work, we perform extensive numerical experiments, where we look at four different surrender profiles, each motivated by empirical research in the literature. Our modeling approaches include the logistic regression, tree based classifiers and neural networks, each in a bagged and a boosted version. The results generally indicate a highly practical performance, where XGBoost is the superior model across all surrender profiles. During the evaluation we place a particular focus on bias and variance, which we compute explicitly by accessing the latent, true surrender probability of each contract. These latent model assessments are additionally compared to evaluations based on observable quantities. With a view to low bias, our results indicate a tradeoff between accurate label prediction for rare events, such as surrender, and a sound estimation of the true surrender probabilities. We numerically affirm earlier findings in the literature that common resampling techniques can indeed improve frequentistic evaluations of our classifiers, as e.g. the F_1 -score. However, our theoretical and numerical results also show that this comes along

with a significant bias of the predicted surrender probabilities. Hence, resampling severely skews the underlying risk and is impractical e.g. with regard to a value-at-risk assessment of surrender risk.

Further, we discuss that each observed surrender event is a realization of a distinct conditional random variable. Therefore, the variance of the latent errors of a model is significantly different to the variance perceived by its predictions. To promote sound model evaluation, that also factors in the uncertainty of predicted surrender probabilities, we consult the central limit theorem of Lindeberg-Feller, which drops the assumption of random variables being identically distributed. Thereby, we derive practical confidence bands on mean surrender rates with respect to calendar-time. This allows us to identify poor performance in a going concern perspective, where the composition of a portfolio or the predominant risk drivers might change over time. Based on mean surrender rates and their confidence bands, our experiments in particular highlight that adding a risk buffer to a naive baseline does not cover the surrender risk sufficiently. This observation indicates the importance of time for a practical model evaluation and provides support for a probabilistic, time-series perspective on surrender risk.

Further research should focus on the application of our findings to high-dimensional, real data sets. We are interested in the benefit of confidence bands for mean surrender rates on data sets, where prior analysis was based on frequentistic concepts and the application of resampling. Confidence bands could also be used to monitor if a given model needs to be recalibrated as either the composition of the portfolio or the behaviour of policyholders change. Further, it would be interesting to extend our results by including the loss-given-surrender, or an appropriate deterministic proxy, and thereby evaluate models based on their estimate of the economic capital at risk due to surrender. The presented concept of mean event probabilities and confidence bands is not restricted to surrender or one year time horizons, but is valid for general Bernoulli-type events. Hence, it can also be used to monitor e.g. the quality of a model for expected fraud rates or one-year death events.

Acknowledgements

The author wants to thank his supervisor Christian Weiß for his precious feedback and numerous helpful discussions. Further, the author is grateful to the 'Ministerium für Kultur und Wissenschaft des Landes Nordrhein-Westfalen' for supporting his research by their grant 'FH BASIS 2019' (reference 1908fhb005). All numerical experiments presented in this work were conducted on a server funded by the respective grant.

References

- [1] O. O. Aalen, Ø. Borgan, M. Gail, H. K. Gjessing, K. Krickeberg, J. Samet, A. Tsiatis, and W. Wong. *Survival and Event History Analysis: A Process Point of View*. Statistics for Biology and Health. New York: Springer, 2008.
- [2] M. Aleandri. "Modeling Dynamic Policyholder Behaviour through Machine Learning Techniques". *Submitted to Scuola de Scienze Statistiche* (2017).
- [3] S. Badirli, X. Liu, Z. Xing, A. Bhowmik, K. Doan, and S. S. Keerthi. "Gradient Boosting Neural Networks: GrowNet" (2020). Available on arXiv 2002.07971.
- [4] F. Barsotti, X. Milhaud, and Y. Salhi. "Lapse risk in life insurance: Correlation and contagion effects among policyholders' behaviors". *Insurance: Mathematics and Economics* 71 (2016), 317–331.
- [5] D. Bauer, R. Kiesel, A. Kling, and J. Ruß. "Risk-neutral valuation of participating life insurance contracts". *Insurance: Mathematics and Economics* 39.2 (2006), 171–183.
- [6] A. A. Borovkov. *Probability Theory*. Universitext. London: Springer, 2013.
- [7] T. Burkhart. "Surrender Risk in the Context of the Quantitative Assessment of Participating Life Insurance Contracts under Solvency II". *Risks* 6.3 (2018), 66.

[8] R. R. Cerchiara, M. Edwards, and A. Gambini. "Generalized Linear Models in Life Insurance: Decrements and Risk Factor Analysis Under Solvency II". *18th AFIR Colloquium*. Rome, 2008.

[9] V. Chandola, A. Banerjee, and V. Kumar. "Anomaly detection: ACM Computing Surveys, 41(3), 1-58" (2009).

[10] N. V. Chawla, K. W. Bowyer, L. O. Hall, and W. P. Kegelmeyer. "SMOTE: Synthetic Minority Over-sampling Technique". *Journal of Artificial Intelligence Research* 16 (2002), 321–357.

[11] T. Chen and C. Guestrin. "XGBoost: A Scalable Tree Boosting System". *Proceedings of the 22nd ACM SIGKDD International Conference on Knowledge Discovery and Data Mining*. 2016, 785–794.

[12] DAV. *Herleitung der Sterbtafel DAV 2008 T für Lebensversicherungen mit Todesfallcharakter*. Ed. by Deutsche Aktuarvereinigung e.V. https://aktuar.de/unsere-themen/lebensversicherung/sterbtafeln/2018-10-05_DAV-Richtlinie_Herleitung_DAV2008T.pdf. Accessed: 2020-06-29.

[13] D. C. Dickson, M. R. Hardy, and H. R. Waters. *Actuarial Mathematics for Life Contingent Risks*. International Series on Actuarial Science. Cambridge University Press, 2009.

[14] R. Durrett. *Probability: Theory and examples*. 4th ed. Cambridge University Press, 2010.

[15] M. Eling and D. Kiesenbauer. "What Policy Features Determine Life Insurance Lapse? An Analysis of the German Market". *The Journal of Risk and Insurance* 81.2 (2014), 241–269.

[16] M. Eling and M. Kochanski. "Research on lapse in life insurance: what has been done and what needs to be done?" *The Journal of Risk Finance* 14.4 (2013), 392–413.

[17] C. Elkan. "The Foundations of Cost-Sensitive Learning". In *Proceedings of the Seventeenth International Joint Conference on Artificial Intelligence* 2001 (2001), 973–978.

[18] European Comission. *QIS5 Technical Specifications*. 2010.

[19] T. Fawcett. "An introduction to ROC analysis". *Pattern Recognition Letters* 27.8 (2006), 861–874.

[20] J. P. Fine and R. J. Gray. "A Proportional Hazards Model for the Subdistribution of a Competing Risk". *Journal of the American Statistical Association* 94.446 (1999), 496–509.

[21] C. Führer and A. Grimmer. *Einführung in die Lebensversicherungsmathematik*. Karlsruhe: Verlag Versicherungswirtschaft, 2006.

[22] Ke. G., Q. Meng, T. Finley, T. Wang, W. Chen, W. Ma, Q. Ye, and T. Liu. "LightGBM: A Highly Efficient Gradient Boosting Decision Tree". *NIPS*. 2017.

[23] GDV. *Statistical Yearbook of German Insurance 2018*. GDV, 2019.

[24] P. Glasserman. *Monte Carlo methods in financial engineering*. New York: Springer, 2010.

[25] I. Goodfellow, Y. Bengio, and A. Courville. *Deep Learning*. MIT Press, 2016.

[26] T. Hastie, R. Tibshirani, and J. H. Friedman. *The elements of statistical learning: Data mining, inference, and prediction*. Second edition. New York: Springer, 2017.

[27] V. Hodge and J. Austin. "A Survey of Outlier Detection Methodologies". *Artificial Intelligence Review* 22(2) (2004), 85–126.

[28] M. Kiermayer and C. Weiβ. "Grouping of contracts in insurance using neural networks". *Scandinavian Actuarial Journal* 0.0 (2020), 1–28.

[29] D. Kiesenbauer. "Main Determinants of Lapse in the German Life Insurance Industry". *North American Actuarial Journal* 16.1 (2012), 52–73.

[30] G. King and L. Zeng. "Logistic Regression in Rare Events Data". *Political Analysis* 9.2 (2001), 137–163.

[31] D. Kingma and J. Ba. "Adam: A Method for Stochastic Optimization". *International Conference on Learning Representation* (2015).

[32] A. Klenke. *Probability Theory*. London: Springer, 2014.

[33] A. Kling, F. Ruez, and J. Ruß. "The impact of policyholder behavior on pricing, hedging, and hedge efficiency of withdrawal benefit guarantees in variable annuities". *European Actuarial Journal* 4.2 (2014), 281–314.

[34] A. W. Kolkiewicz and K. S. Tan. “Unit-Linked Life Insurance Contracts with Lapse Rates Dependent on Economic Factors”. *Annals of Actuarial Science* 1.1 (2006), 49–78.

[35] Federal Ministry of Labour and Social Affairs. *Old-age pensions*. <https://www.bmas.de/EN/Our-Topics/Pensions/old-age-pensions.html>. Accessed: 2019-06-27.

[36] S.-H. Li, D. C. Yen, W.-H. Lu, and C. Wang. “Identifying the signs of fraudulent accounts using data mining techniques”. *Computers in Human Behavior* 28.3 (2012), 1002–1013.

[37] S. Loisel and X. Milhaud. “From deterministic to stochastic surrender risk models: Impact of correlation crises on economic capital”. *European Journal of Operational Research* 214.2 (2011), 348–357.

[38] S. Loisel, P. Piette, and J. Tsai. “Applying economic measures to lapse risk management with machine learning approaches” (2019). Available at arXiv 1906.05087.

[39] M. Maalouf and M. Siddiqi. “Weighted logistic regression for large-scale imbalanced and rare events data”. *Knowledge-Based Systems* 59 (2014), 142–148.

[40] X. Milhaud and C. Dutang. “Lapse tables for lapse risk management in insurance: a competing risk approach”. *European Actuarial Journal* 8.1 (2018), 97–126.

[41] X. Milhaud, S. Loisel, and V. Maume-Deschamps. “Surrender Triggers in Life Insurance: Classification and Risk Predictions”. *Bulletin Français d'Actuariat* 22.11 (2011), 5–48.

[42] C. Phua, V. Lee, K. Smith, and R. Gayler. “A Comprehensive Survey of Data Mining-based Fraud Detection Research” (2012). Available on arXiv 1009.6119.

[43] F. Provost and T. Fawcett. “Robust Classification for Imprecise Environments”. *Machine Learning* 42.3 (2001), 203–231.

[44] G. Rubino and B. Tuffin. *Rare event simulation using Monte Carlo methods*. Chichester: Wiley, 2009.

[45] R. E. Schapire and Y. Singer. “Improved Boosting Algorithms Using Confidence-rated Predictions”. *Machine Learning* 37.3 (1999), 297–336.

[46] C. Seiffert, T. M. Khoshgoftaar, J. van Hulse, and A. Napolitano. “Mining Data with Rare Events: A Case Study”. *19th International Conference on Tools with Artificial Intelligence*. 2007, 132–139.

[47] M. Sokolova and G. Lapalme. “A systematic analysis of performance measures for classification tasks”. *Information Processing & Management* 45.4 (2009), 427–437.

[48] J. Wakefield. *Bayesian and Frequentist Regression Methods*. New York: Springer, 2013.

[49] B. C. Wallace, K. Small, C. E. Brodley, and T. A. Trikalinos. “Class Imbalance, Redux”. *IEEE 11th International Conference on Data Mining*. 2011, 754–763.

[50] G. M. Weiss. “Mining with rarity”. *ACM SIGKDD Explorations Newsletter* 6.1 (2004), 7–19.

[51] G. M. Weiss and F. Provost. “The effect of class distribution on classifier learning”. PhD thesis. San Diego: University of California, 2001.

[52] Lu Yu, Jiang Cheng, and Tzuting Lin. “Life insurance lapse behaviour: evidence from China”. *The Geneva Papers on Risk and Insurance - Issues and Practice* 44.4 (2019), 653–678.

A Appendix

A.1 Proofs

Proof of Proposition 1. In order to apply the central limit theorem of Lindeberg-Feller, it remains to show that the Lindeberg condition holds, see Theorem 15.43 in [32]. Hence, for all $\delta > 0$ we have to show that

$$L_N(\delta) := \frac{1}{\sigma^2(S_N)} \sum_{i=1}^N \mathbb{E} [(Z_i - p(1|x_i))^2 \mathbb{1}_{\{|Z_i - p(1|x_i)| > \delta \sigma(S_N)\}}] \xrightarrow[N \rightarrow \infty]{} 0. \quad (15)$$

Observe that $|Z_i - p(1|x_i)|$ is bounded, while $\sigma(S_N)^2 = \sum_{i=1}^N p(1|x_i)(1 - p(1|x_i)) \xrightarrow[N \rightarrow \infty]{} \infty$, given that $p(1|x_i) \in [\varepsilon, 1 - \varepsilon]$ for all $i \in \mathbb{N}$. Hence, for every $\delta > 0$ there is $\bar{N}_\delta \in \mathbb{N}$ such that $|Z_i - p_{x_i}| < \delta \sigma(S_N)$, for all $N > \bar{N}_\delta$ and for all $i \in \mathbb{N}$. Therefore, the sum in (15) contains at most \bar{N}_δ bounded summands and we conclude $L_N(\delta) \xrightarrow[N \rightarrow \infty]{} 0$. \square

Proof of the Corollary 1. By Lemma 1, we know

$$\frac{1}{\sigma(S_N)} \sum_i Z_i - p(1|x_i) \xrightarrow{d} \mathcal{N}(0, 1). \quad (16)$$

Then, for large values of N

$$1 - \frac{\alpha}{2} = \mathbb{P}\left(\frac{1}{N} \sum_i Z_i \leq z\right) \approx \Phi\left(\frac{Nz - \sum_i p_{x_i}}{\sqrt{\sum_i p(1|x_i)(1 - p(1|x_i))}}\right), \quad (17)$$

holds, and therefore

$$z \approx \frac{1}{N} \sum_i p(1|x_i) + \Phi^{-1}\left(\frac{\alpha}{2}\right) \frac{\sqrt{\sum_i p(1|x_i)(1 - p(1|x_i))}}{N}. \quad (18)$$

Let $\hat{p} : x \mapsto \hat{p}(1|x)$ describe the estimator for the true Bernoulli probabilities $p : x \mapsto p(1|x)$. Then, substituting $\frac{1}{N} \sum_i p(1|x_i)$ by its estimate $\frac{1}{N} \sum_i \hat{p}(1|x_i)$ and the standard deviation $\sigma(S_N) = \sqrt{\sum_i p(1|x_i)(1 - p(1|x_i))}$ by its asymptotically unbiased sample estimate $\hat{\sigma}(S_N) = \sqrt{\frac{N}{N-1}} \sqrt{\sum_i \hat{p}(1|x_i)(1 - \hat{p}(1|x_i))}$ yields the statement. \square

Proof of Lemma 1. Using the decomposition proposed in Theorem 1 and $\hat{p}^S(y=1) > \hat{p}(y=1)$ yields

$$\begin{aligned} \hat{p}^S(1|x) &= \hat{p}(1|x) \frac{\hat{p}^S(y=1)(1 - \hat{p}(y=1))}{\hat{p}(y=1)(1 - \hat{p}(1|x)) + \hat{p}^S(y=1)(\hat{p}(1|x) - \hat{p}(y=1))} \\ &> \hat{p}(1|x) \frac{\hat{p}^S(y=1)(1 - \hat{p}(y=1))}{\hat{p}^S(y=1)(1 - \hat{p}(1|x)) + \hat{p}(1|x) - \hat{p}(y=1)} \\ &= \hat{p}(1|x). \end{aligned}$$

\square

A.2 Simulation of endowment policies.

We present the simulation scheme for the portfolio at the initial calendar year. New business at subsequent calendar years is simulated analogously with the condition that the currently elapsed duration equals zero. Let us denote an arbitrary contract $X = (X^{(1)}, \dots, X^{(n)})$ with $n = 8$. The features correspond to the calendar year ($X^{(1)}$), the current age of the policyholder ($X^{(2)}$), the face amount of the contract ($X^{(3)}$), the duration ($X^{(4)}$), the elapsed duration ($X^{(5)}$), the remaining duration ($X^{(6)}$), the frequency of premium payments ($X^{(7)}$) and the annual amount of premium payments ($X^{(8)}$). For the simulation we use a Pearson gamma distribution $\Gamma_{\alpha, \lambda}$ with shape $\alpha > 0$ and rate $\lambda > 0$, see [6], as well as the uniform distribution $\mathcal{U}(0, 1)$. The gamma distribution provides a flexible, right skewed distribution. For a random variable $\zeta \sim \Gamma_{\alpha, \lambda}$ the expectation and variance of ζ are given by

$$\mathbb{E}(\zeta) = \frac{\lambda}{\alpha}, \quad \text{Var}(\zeta) = \frac{\lambda}{\alpha^2}.$$

In [40], we find 34% of policyholders to be of ages 0-34, respectively 34.04% and 18.5% of ages 35-54 and 55-84. This indicates a right-skewed distribution for a policyholder's age. Further, most lapse events, including maturity, are indicated to occur within 15 years. The authors in [40] also report roughly 25% annual premium payments, 60% infra annual and 15% supra annual payments. The annual premium amount is reported to be highly right-skewed. We calibrate the marginal distributions of features $X^{(i)}$, $i > 1$, to closely imitate these statistics. We define

$$\begin{aligned} X^{(2)} &\sim \Gamma_{5.5, 6.8^{-1}}, & X^{(4)} &\sim 5 + \Gamma_{5, 1.5^{-1}}, \\ X^{(3)} &\sim 5'000 + \Gamma_{4, 2'000^{-1}}, & X^{(5)} &\sim \min(X_4 \cdot \mathcal{U}(0, 1), X_2). \end{aligned}$$

As we do not permit negative ages at the underwriting of the contract, the elapsed duration $X^{(5)}$ is engineered to not exceed the current age. The remaining duration $X^{(6)}$ of a contract is then obtained deterministically by $X^{(6)} := X^{(4)} - X^{(5)}$. Further, the premium frequency $X^{(7)}$ is a categorical variable which mirrors [40] with

$$X^{(7)} = \begin{cases} \text{upfront} & , \text{ with prob. 0.15} \\ \text{annual} & , \text{ with prob. 0.25} \\ \text{monthly} & , \text{ with prob. 0.6} \end{cases}.$$

Last, we determine the fair premium by the equivalence principle in [13, 21] annualize it linearly based on the premium frequency and the number of remaining premium payments up to maturity, respectively at most up to the last premium payment at retirement, i.e. at age 67. The resulting annual premium $X^{(8)}$ is then used to calibrate the parameters of the face amount $X^{(3)}$. The reported parametrization of $X^{(3)}$ leads to an annual, mean premium of 1'300 EUR, which inherits the right-skew from $X^{(3)}$.

A.3 Surrender profiles

All surrender profiles used for the experiments in this work are based on findings in the literature, see [8, 15, 41], which all employ logistic regressions and report quantitative results on $\beta_x^{(i)} x^{(i)}$ for surrender. Empirical results in [41] are obtained on endowment insurance contracts in Spain, while [8] and [16] consider life insurance contracts of multiple types in the Italian and German market. Given surrender behaviour on various markets, we do not aim to combine them to a holistic surrender model. Instead we create multiple surrender profiles that capture a variety of the observed risk characteristics. To plausibly combine multiple risk drivers $\beta_x^{(i)} x^{(i)}$ we adjust the baseline risk β_0 such that the observed mean surrender rates of each risk profile fall into practical ranges of 0.01 to 0.05.

Profiles 1 and 2. In [41] the authors use odd ratios to identify quality and severity of risk drivers for endowment insurance products. To compute the odd ratio of a single feature i , we take for two contracts x and \tilde{x} , which only differ in feature i , i.e. $x^{(j)} = \tilde{x}^{(j)}$ for $j \neq i$. The odd ratio is then computed by

$$\frac{p(1|x)/(1-p(1|x))}{p(1|\tilde{x})/(1-p(1|\tilde{x}))} = \exp\{\beta_x^{(i)} x^{(i)} - \beta_{\tilde{x}}^{(i)} \tilde{x}^{(i)}\}. \quad (19)$$

If we set $\beta_{\tilde{x}}^{(i)} \tilde{x}^{(i)} := 0$ as the baseline risk of feature i , we can extract $\beta_x^{(i)} x^{(i)}$ for all features i . Consequently, we construct surrender profile 1 based on empirical odd ratios and surrender profile 2 based on modeled odd ratios, both are reported in [41]. The risk drivers are restricted to the current age of the policyholder, the elapsed duration of the contract, the frequency of premium payments, i.e. monthly, annually or as a lump sum, and the annualized premium amount. Due to data confidentiality in [41], the actual premium amounts are omitted. Hence, we transfer the odd ratio for the savings premium in [41] to our meta model by assuming the indicated jumps to occur at plausible levels of 1'000 EUR resp. 2'000 EUR.

Profiles 3 and 4. We keep the the effect of the elapsed duration and the annualized premium amount fixed to the values in surrender profile 2. For the premium frequency, as well as the remaining duration we employ results in [15], including regression coefficient estimated on a per contract basis. These results indicate a reduced risk of surrender for single premium payments and an increased risk for a high remaining duration. Further, in [8] we find a mitigating effect of mid-range ages, as well as an increased surrender activity for contracts with a duration of less than 10 years, both reported in the form of $\beta_x^{(i)} x^{(i)}$. This completes surrender profile 3. Lastly, for surrender profile 4 we additionally include the calendar year as a risk driver and impose coefficients reported in [8] for the years 1991 up to 2007. The calendar year can be viewed as a proxy for the economic environment or alternatively as noise to the surrender activity, as input variables x in our data do not include economic features.

A.4 Figures

		predicted label	
		$\hat{y} = 1$	$\hat{y} = 0$
actual label	$y = 1$	True Positive (TP)	False Negative (FN)
	$y = 0$	False Positive (FP)	True Negative (TN)

Figure 6: Confusion Matrix

A.5 Tables

Measure	Formula	Interpretation
Accuracy	$\frac{TP+TN}{TP+FP+FN+TN}$	Overall share of correctly classified labels
Precision	$\frac{TP}{TP+FP}$	Share of correct label predictions $\hat{y} = 1$
Recall ⁵	$\frac{TP}{TP+FN}$	Share of correctly classified data with $y = 1$
Specificity	$\frac{TN}{FP+TN}$	Share of correctly classified data with $y = 0$
False positive rate	$\frac{FP}{FP+TN}$	Share of misclassified data with $y = 0$
F_β -score	$\frac{(1+\beta) \cdot \text{recall} \cdot \text{precision}}{\beta^2 \cdot \text{recall} + \text{precision}}$	Weighted balance ($\beta > 0$) between recall and precision

Table 3: Measures for binary classification, adapted from [47].

profile	$ \mathcal{D}_{\text{train}} $	imbalance	RUS	SMOTE	$ \mathcal{D}_{\text{test}} $	imbalance
0	189285	0.0290	10966	367604	75414	0.0454
1	212978	0.0165	7042	418914	81113	0.0131
2	217515	0.0201	8738	426292	89671	0.0162
3	216734	0.0210	9082	424386	89105	0.0159

Table 4: Overview of number of 1-year observations and imbalance in the training and test set of all surrender profiles. Additionally, we report the number of observations in a perfectly balanced training set resulting from random-undersampling (RUS) and SMOTE-resampling.

Profile	Logist. Regr.	Random Forest	XGBoost	NN - bagging	NN - boosting
0	215	10	3	1245	3152
1	177	12	4	1392	3512
2	280	13	4	2710	3411
3	465	12	5	1589	3160

(a) No resampling.

Profile	Logist. Regr.	Random Forest	XGBoost	NN - bagging	NN - boosting
0	13	23	31	3333	15353
1	10	27	32	8992	18975
2	26	31	35	7594	21738
3	29	30	35	10114	24501

(b) Random undersampling.

Profile	Logist. Regr.	Random Forest	XGBoost	NN - bagging	NN - boosting
0	621	23	8	2937	13915
1	1452	29	11	7756	18133
2	4045	31	13	8598	22152
3	5952	27	13	9937	27057

(c) SMOTE-resampling.

Table 5: Training-times (in sec.) of the discussed classifiers for surrender profiles 1-4 and types of resampling.